The Pennsylvania State University
The Graduate School

ON SOME EMERGING ISSUES OF POWER SYSTEMS WITH INVERTER-BASED RESOURCES

A Thesis in
Electrical Engineering
by
Baljeet Singh

Submitted in Partial Fulfillment
of the Requirements
for the Degree of

Master of Science

May 2024

The thesis of Baljeet Singh was reviewed and approved by the following:

Nilanjan Ray Chaudhuri
Associate Professor of Electrical Engineering
Thesis Advisor

Yan Li
Assistant Professor of Electrical Engineering
Charles H. Fetter Endowed Fellow Assistant Professor

Yunting Liu
Assistant Professor of Electrical Engineering

Madhavan Swaminathan
Professor of Electrical Engineering
Department Head and William E. Leonhard Professor

Abstract

The thesis is focused on fast time-domain simulation of power systems with inverter-based resources (IBRs) and impact of IBRs on distance protection.

The detailed dynamic model of power system in terms of differential and algebraic equation provides an access to study the behavior of oscillations in case of disturbances, before achieving the steady-state value. However, when the goal of study is to obtain the equilibrium only, it is less effective, as the dynamic simulations take time. Therefore, an approach for fast simulation based on Backward-Euler method (BEM) has been presented in this thesis with an ability to provide an average response of dynamic model of power systems with IBRs. BEM has the ability to perform simulations with large step-size and proven to be useful in long-term simulations. In this thesis, a power system with integration of a grid-following converter (GFLC) and a synchronous generator (SG) is used as the test system. The differential equations of the system are represented by converter control loops and swing equation of SG in the state-space form, and the power flow equations in the network represents algebraic equations of the dynamic model. The implicit numerical integration method, Trapezoidal method (TM) is used to provide the ground truth of the dynamic model. The results obtained from simulations with BEM is compared to that of TM and the proposed approach is able to provide similar end-results to that of ground truth with reduced simulation time. Thus, the proposed approach will potentially enable dynamic security assessment of a large power system with massive number of IBRs.

Moreover, the thesis also tests a relay design used in conventional power systems for protection of power systems with IBRs. The relay operation is based on distance protection. The distance protection uses the ratio of voltage to current or impedance of transmission line as viewed from the relay location as a parameter for the functioning of relay. The relay model was tested in MATLAB/Simulink first with SG and then with the Photovoltaic (PV) generation acting as the IBR, which is tied to AC power grid for synchronization. In case of short-circuit faults, IBRs are not able to provide sufficient short circuit current as compared to SGs. The simulation results show that relays designed for conventional power systems may overreach in presence of IBRs.

Table of Contents

List of Figures

List of Tables

List of Symbols

v_{dq}	Voltage magnitude of bus connected to Grid-following converter (GFLC)
E_q	Voltage magnitude of bus connected to synchronous generator (SG)
E'	Magnitude of voltage behind transient reactance
v_d	Direct-axis voltage of GFLC
v_q	Quadrature-axis voltage of GFLC
i_d	Direct-axis current of GFLC
i_q	Quadrature-axis current of GFLC
δ_g	Rotor angle
θ_{pll}	Angle of $d-q$ reference frame of Phase-locked loop (PLL) with respect to real-imaginary reference frame
θ_g	Voltage angle of bus connected SG
θ_c	Voltage angle of bus connected to GFLC
ω_{pll}	Angular speed of $d-q$ reference frame of Phase-locked loop
ω_s	Synchronous speed
ω_g	Rotor speed
P_m	Mechanical power input to SG
P_c	Real power input from GFLC
Q_c	Reactive power input from GFLC
P_g	Real power input from SG
Q_g	Reactive power input from SG

P_{lc} Load connected to GFLC bus

P_{lg} Load connected to SG bus

X Transmission line reactance

X'_d Transient reactance of SG

X_l Leakage reactance of transformer

x_{pll} PLL controller state

x Outer voltage control loop controller state

d_{pg} Droop coefficient of governor control of SG

R_{pc} Droop coefficient of power-frequency droop controller

K_{ip} Integral gain of power-frequency droop controller

K_i Integral gain of outer voltage control loop

K_p Proportional gain of outer voltage control loop

K_i^{pll} Integral gain of PLL

K_p^{pll} Proportional gain of PLL

K_D Damping coefficient

H_g Inertia constant

τ_v time-delay to voltage magnitude v_{dq}

τ_i time-delay to i_d and i_q

τ_g time-delay in governor's output

P_c^* Real power reference of GFLC

Q_c^* Reactive power reference of GFLC

P_g^* Real power reference of SG

i_d^* Direct-axis reference current of GFLC

i_q^* Quadrature-axis reference current of GFLC

Acknowledgments

First of all, I would like express my sincere gratitude to my research advisor Dr. Nilanjan Ray Chaudhuri for showing his trust in me and providing me this opportunity and constantly guiding me throughout the research. Meeting with him and discussing the concepts related to power systems domain broadened the horizon of my knowledge in this particular field. His emotional support and motivation to try solve the problem helped me acheive another milestone in my life.

I would also like to thank my lab mates at Power Systems Lab- Lilan Karunaratne, Soumyajit Gangopadhyay, Fiaz Hossain for their guidance and support. Being my seniors, they guided me selflessly in using several applications and technical writings.

Further, I extent my appreciation towards the committee members Dr. Yan Li and Dr. Yunting Liu for being a part of my committee and sharing their insights towards completion of thesis.

I would like to thank my friend and family for their motivation in lifting up my spirit. Their constant support made me do better whenever I was not making any progress.

I am grateful to the National Science Foundation (NSF) for the funding support under award ECCS 1836827. Please note that the findings and the conclusions of this thesis do not necessarily reflect the view of the funding agency.

Without the support of people I mentioned and others I forgot to mention, I don't think I would have been able to present my thesis.

Chapter 1 Introduction

1.1 Introduction

Electricity has became one of the utmost requirements of today's generation. In this era, it is unimaginable to have a life without electricity. Without any doubt, electricity has reduced the time and human efforts to do specific tasks. However, a major portion of the electric power is generated with fossil-fuels, which pollutes the environment. Due to climate change issues, it has become very critical to trace emission of pollutants from power generating station into the atmosphere. Therefore, renewable energy resources are being considered the future of power generation. However, with the increase in penetration of renewable energy resources, power grids are facing new challenges, which are discussed in the later sections. In this thesis, some major problems related to the power systems with renewable resources are accounted and their possible solutions are discussed along with it.

1.2 Need of inverter-based resources (IBRs)

For many years, power systems consisted of centralized unidirectional system with three subsystems in which power was generated by generating units, which are thermal, hydro and nuclear power plant followed by transmission over long distance lines and delivered to consumers by distribution systems [1] - [2]. Figure 1.1 [3] provides an illustration of the conventional power system.

However, the traditional generating unit requires fossil-fuels to generate electricity which is present in limited amount, along with polluting the environment. With the production of electricity, it emits greenhouse gases in the environment. These gases

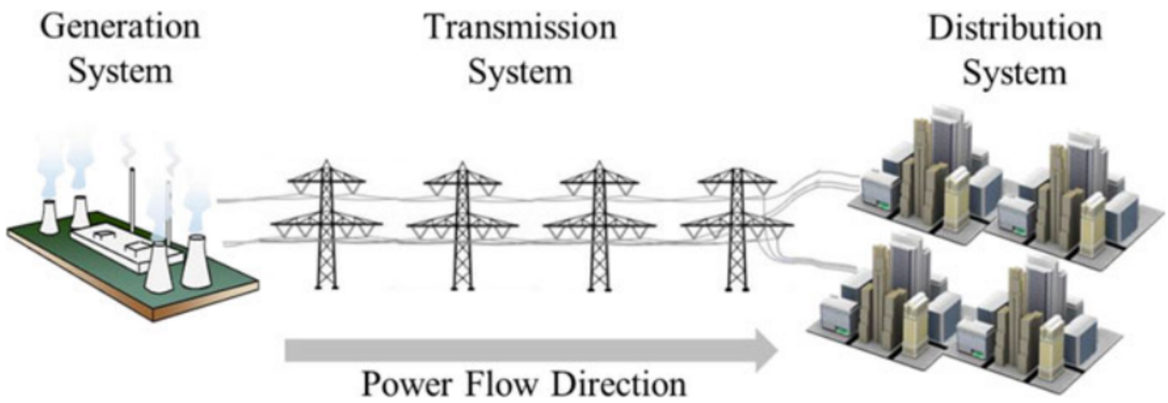

Figure 1.1. Conventional power system.

are continuously making the planet warmer by tapping heat. Figure 1.2 [4] shows the greenhouse gas emissions related to different sectors in United States for year 2018.

Electricity sector accounted for almost 27% of overall greenhouse gas emissions in the United States for year 2018 as represented by pie chart in Fig. 1.2. Approximately 63% of the electricity in United States is produced by thermal power plants by burning coal and natural gas [5]. To avoid the detrimental affects caused by greenhouse gas emission, there is a need for a promising alternative to generate electricity. Furthermore, the conventional power system is considered outdated and vulnerable to cascading failures due to its dependency only on the centralized generating station [3].

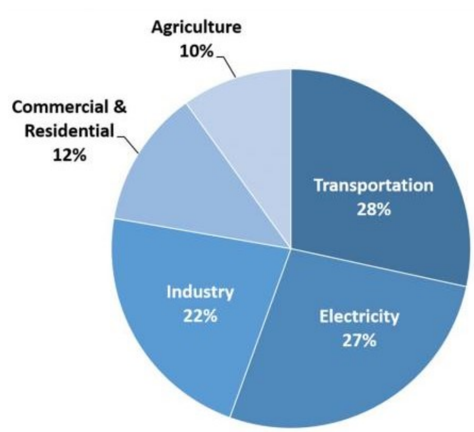

Figure 1.2. Greenhouse gas emissions by economic sector in 2018.

Climate change is becoming a widespread concern across the globe due to which renewable sources of energy, such as solar energy, wind energy etc. are continuously replacing conventional thermal generation units to contribute towards energy sustainability.

Figure 1.3 [4] shows the emission and trends for greenhouse gases from year 1990 to 2018.

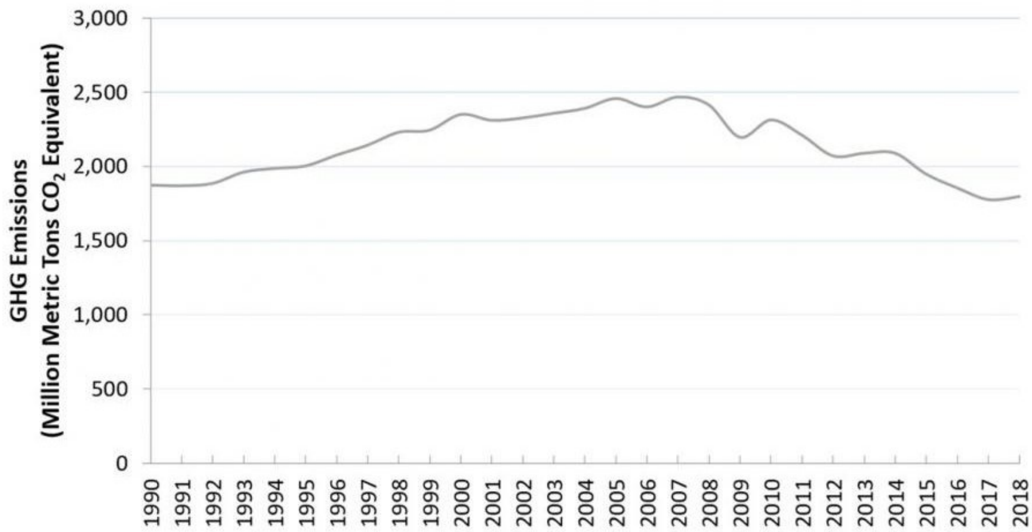

Figure 1.3. Greenhouse gas emissions from electricity.

It can be seen from the Figure 1.3 that with the introduction of renewable energy resources, the carbon emissions tends to decrease considerably, which was 4.1% less than that of year 1990.

However, the resources requires an additional interface between generation and distribution unit to convert the electricity into standard form as required by the AC system. Therefore, the sources of energy requiring additional power electronics converters are referred as inverter-based resources (IBRs).

1.3 Challenges faced by IBR-dominated power grid

With increasing environmental and sustainability concerns, there is relative increase in penetration of IBRs into the power grid, interfaced to synchronous generators (SG), causing a number of challenges. The reason for this problem is due to uncertain and variable nature of power generation from IBRs and its non-synchronous or asynchronous interface with the power grid [6].

Moreover, implementation of fast-acting controllers in power electronics interface is continuously depleting the inertia of the system, thus making it less resilient or more vulnerable to the power system dynamics. The major concern with low-inertia power systems is their elevated rate of change of frequency (RoCoF) [7].

In addition, increased penetration of IBRs to power grid, increase total harmonic distortion (THD) of current and voltage waveforms, due to super-fast switching of the inverters, degrading the power quality of the system [8].

Renewable energy resources, such as photovoltaic and wind generation, which highly depend on environmental factors, cause voltage fluctuations in power grid. To resolve this problem, voltage regulators and load tap changers are employed frequently, thereby reducing their life-cycle [9].

Control-loops of IBRs operate on relatively high bandwidths to control their output voltages and currents. The control-loops may lead to high-frequency oscillations and super-synchronous oscillations due to unplanned interaction between the wind turbine generators and IBRs. Additionally, fast-acting power electronics switches in the IBRs and the filter circuits can also engage these high-frequency oscillation modes [10].

Blackstart is a vital operation in case the power system collapses. It is referred as restoration of the electrical substation without the dependence on the external power source. This service is only limited to grid-forming IBRs. However, grid-forming IBRs providing a blackstart should have high current capability in order to energize the transmission lines and transformers. Also, following a blackstart process, separate sections of the power grid are required to be energized sequentially. With the high penetration of IBRs, each step is a complex data and decision making process. A misstep can cause significant risk to the power system. Moreover, energizing separate elements of power system requires high in-rush currents, subsequently requiring high overcurrent capabilities [10].

Energy resources require real and reactive power ramping capabilities and sufficient control ranges during an island operation. However, in case of IBRs especially Photovoltaic (PV) and wind energy, the power is more dependent on real-time energy resources which are solar energy and wind [10].

1.4 Long-term simulation of power system with IBRs

The dynamic model of power systems is represented in the form of nonlinear differential and algebraic equations (DAEs) [2]. Whenever there is a disturbance in the power system, it experiences transients for a number of cycles before achieving new equilibrium if system is stable, which depends on the state-space model of the power system. Chapter 2 discusses the DAE modeling of the power system with grid-following converter (GFLC) and SG.

In the context of this work, two different numerical methods are used for the purpose of solving DAEs, namely Trapezoidal method (TM) and Backward Euler method (BEM). BEM has the ability to perform fast simulations with large integration time steps by neglecting oscillation. This property of BEM is known as stiff decay [11]. However, we cannot expect large step-size in TM, but in reality TM provides the ground truth of the dynamic model experiencing oscillations [12].

TM is implemented for the purpose of studying transients in the system. This however takes significant amount of time to simulate dynamic models of power systems. In contrast, BEM with its ability to perform large step size, helps in achieving the equilibrium point faster. The integration methods chosen depends on individual's goal. BEM with its ability to utilize large step size, it can be applied in long-term simulation of power systems including cascading failure analysis, where the major requirement is to extract the end of cascade equilibrium condition [11]. Since it is computationally prohibited to apply TM for bulk power system models with large number of IBRs, it is important to explore alternative approaches like BEM. The long-term simulation process and related simulation results are discussed in chapter 3.

1.5 Power system protection with IBRs

Synchronous generators (SGs) have been employed for electricity generation in the conventional power systems. The fault current contribution of the SGs during the short-circuit fault is significantly high compared to nominal current, allowing the protective relays to have a reliable operation and secure the elements of power network. In contrast, integration of IBRs to the conventional system at large scale have posed some new problems in power system protection [13]. During short-circuit conditions, the fault current contribution from IBRs is not as significant as SGs [14], in addition to variable response time of the converter, which considerably depends upon the converter controller, resulting in ineffective or delayed operation of protective relays. Power systems with highly integrated IBRs usually have a limited value of short-circuit current, which is not more than 120% of the rated current [15]. Due to limited value of short-circuit current during the fault, the outer voltage control loop will not operate properly.

With insignificant short-circuit current contribution of power converters and control operations of the power converters, existing relays in the conventional power systems are face challenges in distinguishing between normal operating and fault conditions [16]. Due to which, relay mis-operation may takes place in such systems. Therefore, the relay implemented in conventional power system is tested in presence of IBR to address the issue.

Chapter 4 provides the brief discussion of conventional impedance relays in presence of IBRs.

Chapter 2 | Modeling and simulation of power systems with IBRs

2.1 Introduction

Chapter 1 provides the background of challenges faced by the power system with penetration of IBRs. This chapter presents the formulation of the dynamic model of the power system, considering different elements. The chapter discusses the modeling of GFLC and SG in the network using ordinary differential equations (ODEs). The power balance equations of the system are represented by algebraic equations, thereby leading to a set of DAEs. The state-of-art on the simultaneous approach is also discussed in this chapter to obtain solutions of these DAEs using the trapezoidal method (TM).

2.2 Modeling of GFLCs

GFLCs cannot work in stand-alone condition as it requires an external source of synchronization, i.e., AC grid. The d-axis and q-axis reference currents, i_d^* and i_q^* are given by the power-frequency droop and outer voltage control loops shown in Fig. 2.1 [17] and Fig. 2.2 [18], respectively. The power-frequency droop control works by generating a power reference from deviation of Phase-locked loop (PLL) frequency from synchronous frequency (ω_s - ω_{pll}) followed by scaling through inverse droop coefficient, R_{pc}.

PLL is considered as one of the most important components of GFLCs. Figure 2.3 [19] shows the block diagram of PLL, where the voltage vector of the bus to which GFLC is to be connected is given by $v_{dq}\angle\theta_c$. Here, v_{dq} is given by $\sqrt{v_d^2 + v_q^2}$. The function of PLL is to align the d-axis of the rotating reference frame with the vector $v_{dq}\angle\theta_c$, such that

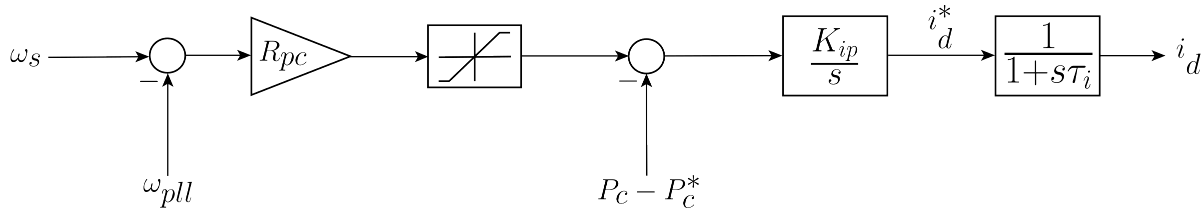

Figure 2.1. Power-frequency droop control.

the q-axis component of the voltage v_q is zero. The deviation of angular frequency of the PLL from a synchronously rotating frame (ω_s - ω_{pll}) is used to generate the reference angle θ_{pll}.

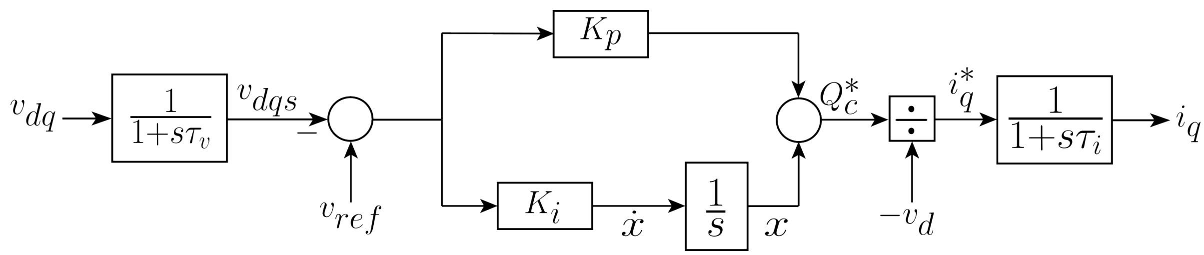

Figure 2.2. Outer voltage control loop.

Figure 2.2 [18] shows the block diagram of PI voltage controller, which is used to generate q-axis reference current, i_q^*. The voltage magnitude v_{dq} acts as the feedback signal to this controller followed by a delay which considers the effect of sensor, communication and filtering delay. The delayed output is then compared with the reference voltage, v_{ref}. The PI controller provides reactive power reference Q_c^*, which is the reactive power delivered by GFLC under steady-state conditions. Assuming that the voltage vector $v_{dq}\angle\theta_c$ is aligned with the d-axis of the PLL under steady-state conditions, making $v_q = 0$. Hence, reactive power reference is given by

$$Q_c^* = -v_d i_q^* \tag{2.1}$$

Further, i_q^* for the steady-state can be obtained from (2.1).

2.2.1 Phasor representation

Figure 2.4 shows the phasor of the voltage at GFLC bus, $v_{dq}\angle\theta_c$ with respect to two different reference frames. The first reference frame is the real-imaginary $(R-I)$ reference frame which is rotating at synchronous speed ω_s. The other reference frame is related to the PLL, which is the $d-q$ reference frame. Suppose the reference frame is leading

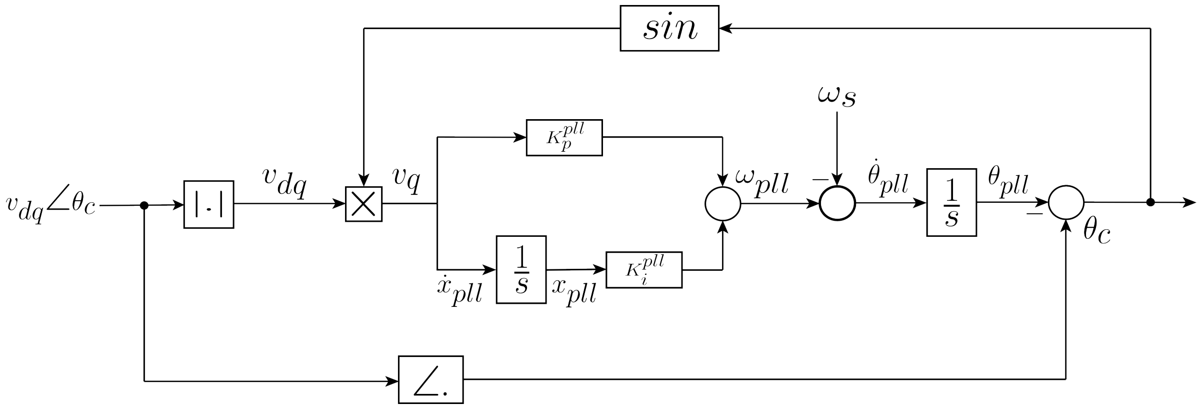

Figure 2.3. Phase-locked loop (PLL).

$R-I$ reference frame by an angle, θ_{pll}. Phasor $v_{dq}\angle\theta_c$ is assumed to be aligned to the d-axis of the $d-q$ reference frame during steady-state conditions, implying $v_q = 0$. The $d-q$ reference frame rotates with the speed equal to synchronous speed (ω_s) during steady-state conditions. Therefore, under steady-state conditions θ_{pll} is a constant. The angle between the vector $v_{dq}\angle\theta_c$ and the $R-I$ reference frame is θ_c.

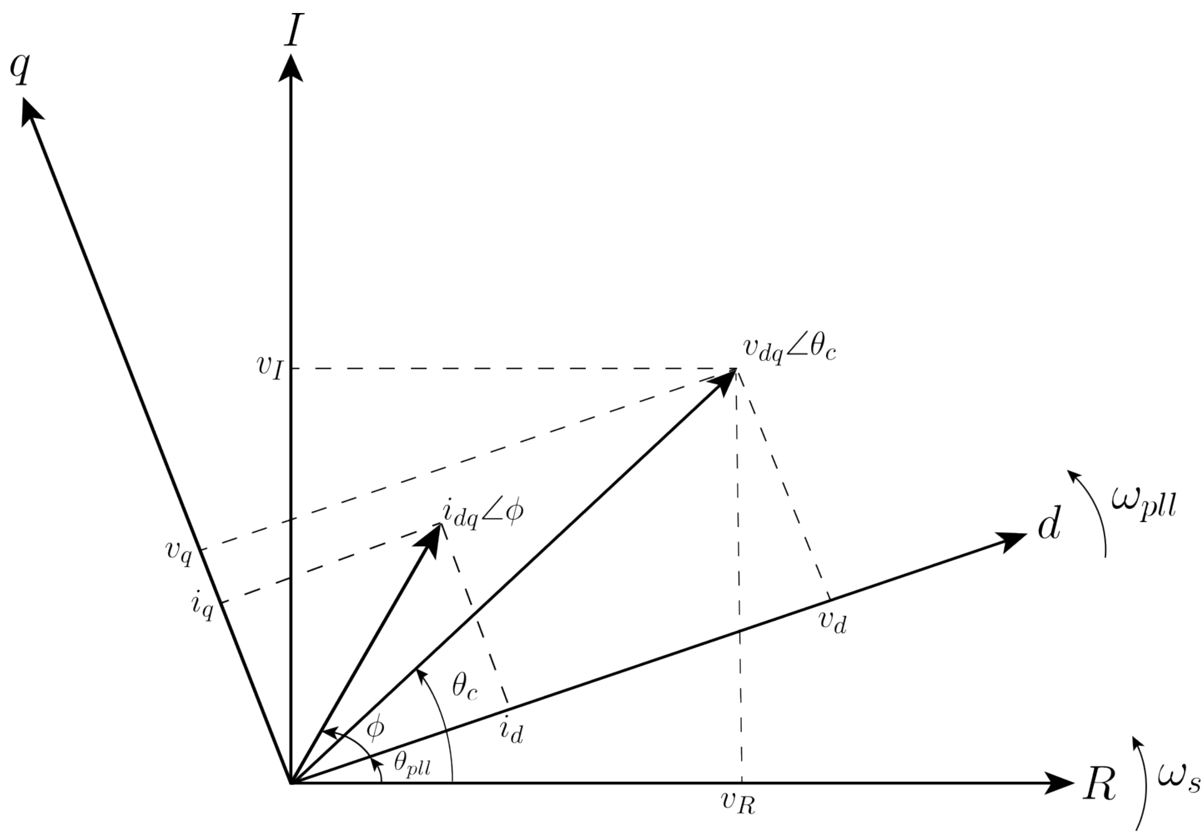

Figure 2.4. Phasor diagram.

2.2.2 State-space representation

The state-space model of GFLC represents the power-frequency droop control (Fig. 2.1), outer voltage control loop (Fig. 2.2) and PLL dynamics (Fig. 2.3). The ODEs resulting from power control can be written as:

$$\dot{i}_d^* = K_{ip}[R_{pc}(\omega_s - \omega_{pll}) + P_c^* - P_c] \tag{2.2}$$

$$\dot{i}_d = \frac{1}{\tau_i}(i_d^* - i_d) \tag{2.3}$$

The ODEs related to outer voltage control loop are represented as:

$$\dot{x} = \frac{K_i}{K_p}(-v_d i_q^* - x) \tag{2.4}$$

$$\dot{v}_{dqs} = \frac{1}{\tau_v}(v_{dq} - v_{dqs}) \tag{2.5}$$

$$\dot{i}_q = \frac{1}{\tau_i}(i_q^* - i_q) \tag{2.6}$$

where, i_q^* is a dependent variable which can be calculated from outer voltage control loop (Fig. 2.2) as:

$$i_q^* = \frac{K_p(v_{ref} - v_{dqs}) + x}{-v_{dq}\cos(\theta_c - \theta_{pll})} \tag{2.7}$$

The PLL dynamics can be written as:

$$\dot{\theta}_{pll} = (K_p^{pll}(v_{dq}\sin(\theta_c - \theta_{pll})) + K_i^{pll}x_{pll}) - \omega_s \tag{2.8}$$

$$\dot{x}_{pll} = v_{dq}\sin(\theta_c - \theta_{pll}) \tag{2.9}$$

From PLL model in Fig. 2.3, it can be seen that

$$\omega_{pll} = K_p^{pll}(v_{dq}\sin(\theta_c - \theta_{pll})) + K_i^{pll}x_{pll} \tag{2.10}$$

In the above mentioned ODEs, P_C is the real power output from the GFLC and it is given by (refer to Appendix for more details)

$$P_c = v_{dq}\cos(\theta_c - \theta_{pll})i_d + v_{dq}\sin(\theta_c - \theta_{pll})i_q \tag{2.11}$$

where, K_i and K_p are the gains for the PI controller of the outer voltage control loop, whereas K_i^{pll} and K_p^{pll} are controller gains for the PLL. The time constants for current and voltage are τ_i and τ_v, respectively.

2.3 Classical model of SG

SGs have been represented by the classical model for the purpose of studying their dynamic behavior, see Fig. 2.5 [2]. Herein, it is considered that the power transfer is lossless, thus all the resistances are neglected. The transient reactance of SGs and the leakage reactance of generating transformer are given by X_d' and X_l, respectively. The voltage behind transient reactance is given by $E'\angle\delta_g$. In classical model, the angle δ_g is used as a measure of rotor angle of SG. During disturbance, the magnitude of this voltage E' remains constant, whereas δ_g changes along with rotor speed ω_s [2]. The voltage of the bus to which SG is connected is given by $E_g\angle\theta_g$.

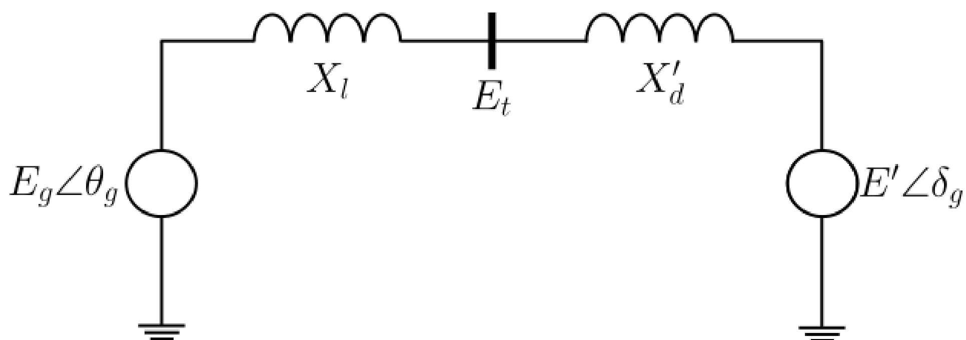

Figure 2.5. Classical model of synchronous generator.

2.3.1 Phasor representation

The vector position of the voltage behind transient reactance of SG, $E'\angle\delta_g$ with respect to synchronously rotating $R-I$ reference frame is shown in Fig. 2.6 [2]. The rotational speed of the rotor ω_g is equal to ω_s under steady-state. The phasor $E'\angle\delta_g$ makes an angle δ_g with the reference frame, and it is constant until a disturbance acts upon the system. The voltage of the bus where SG is connected (E_g) is assumed to be aligned to the real axis of the $R-I$ frame during steady-state.

2.3.2 State-space representation

The SG state-space equations represent the swing equation of the SG and the governor dynamics [2]. Figure 2.7 [20] shows block diagram of the governor operation.

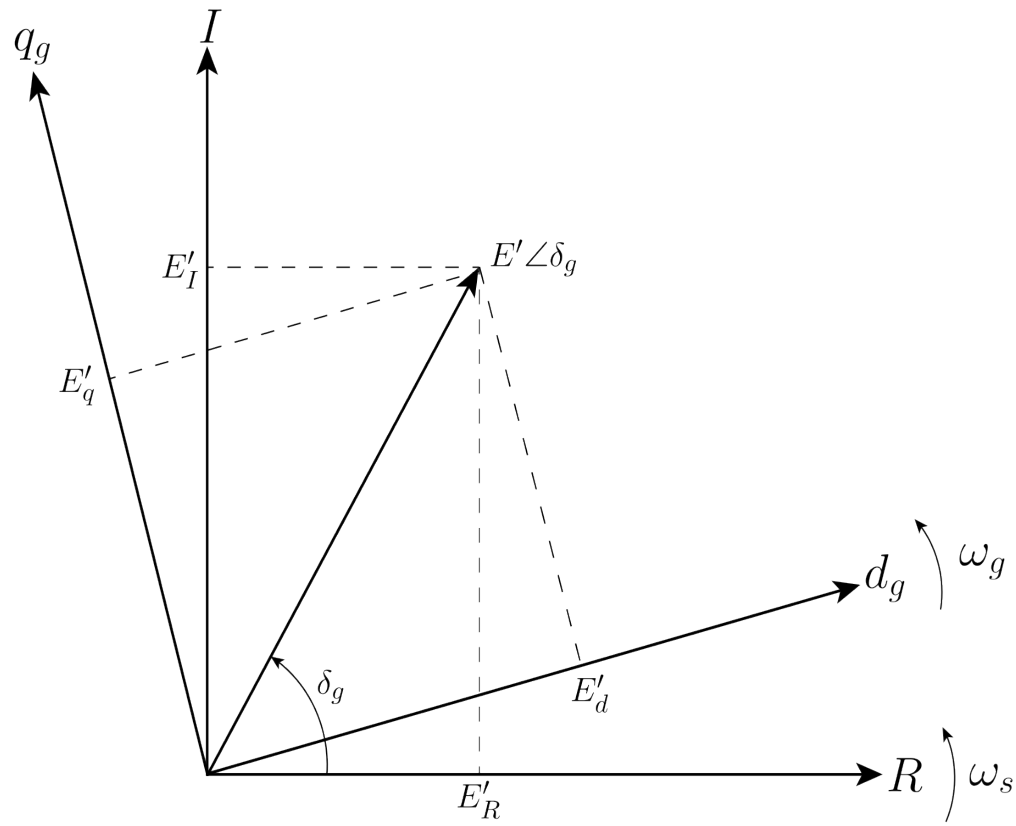

Figure 2.6. Phasor diagram.

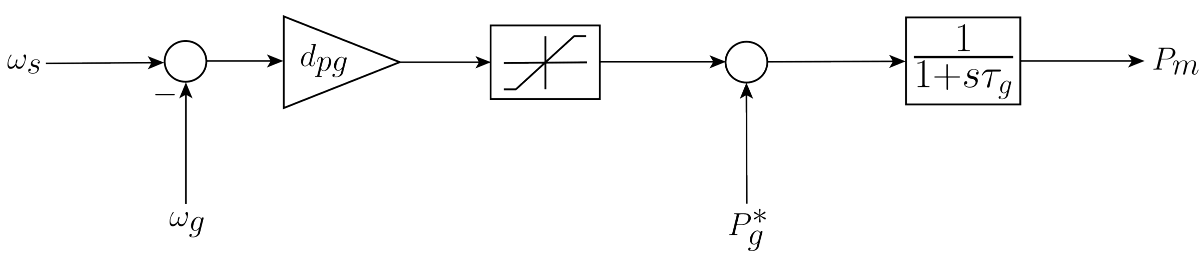

Figure 2.7. Governor control of SG.

Swing equations:

$$\dot{\delta}_g = \omega_g - \omega_s \tag{2.12}$$

$$\dot{\omega}_g = \frac{\omega_s}{2H_g}[P_m - K_D(\omega_g - \omega_s) - P_e] \tag{2.13}$$

Governor dynamics equation:

$$\dot{P}_m = \frac{1}{\tau_g}[P_g^* + d_{pg}(\omega_s - \omega_g) - P_m] \tag{2.14}$$

Herein, ω_s is the reference frequency which is equal to the synchronous frequency. The inverse droop of the governor and the governor's time constant are given by d_{pg} and τ_g, respectively. The damping constant and the inertia constant of the SG are K_D and H_g, respectively.

2.4 System model with GFLC and SG

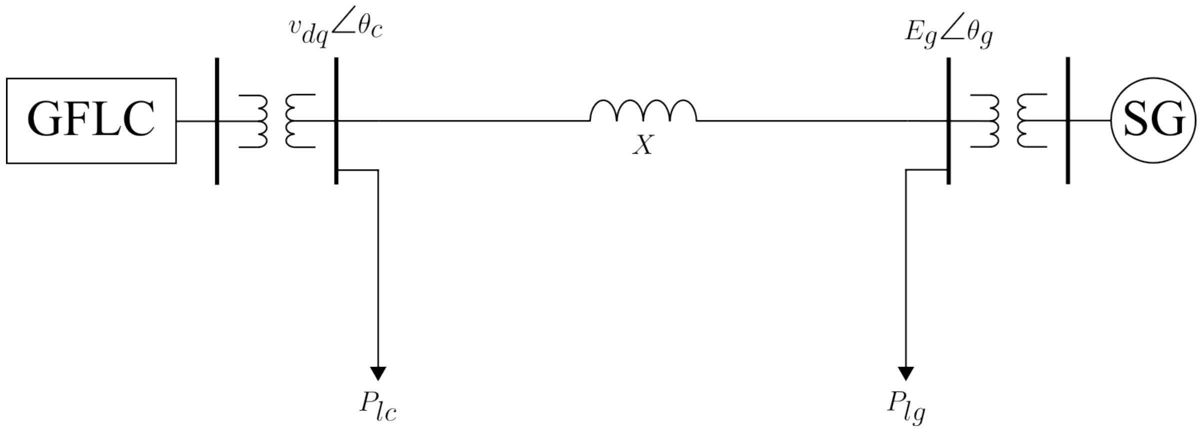

Figure 2.8. Power system under study.

Figure 2.8 shows the power system taken into consideration for the study. In the system, the transmission line is considered to be lossless and purely reactive. There are two loads connected to each bus. The loads connected to the GFLC bus and the SG bus are P_{lc} and P_{lg}, respectively. The loads are assumed to be purely real. Figure 2.9 shows the power system represented by classical model of SG, where X' is the reactance of transmission line between the SG and the bus to which load P_{lg} is connected. In presence of a GFLC in the power system, swing equation in (2.13) is updated as:

$$\dot{\omega}_g = \frac{\omega_s}{2H_g}[P_m + P_c - K_D(\omega_g - \omega_s) - P_{lg} - P_{lc}] \tag{2.15}$$

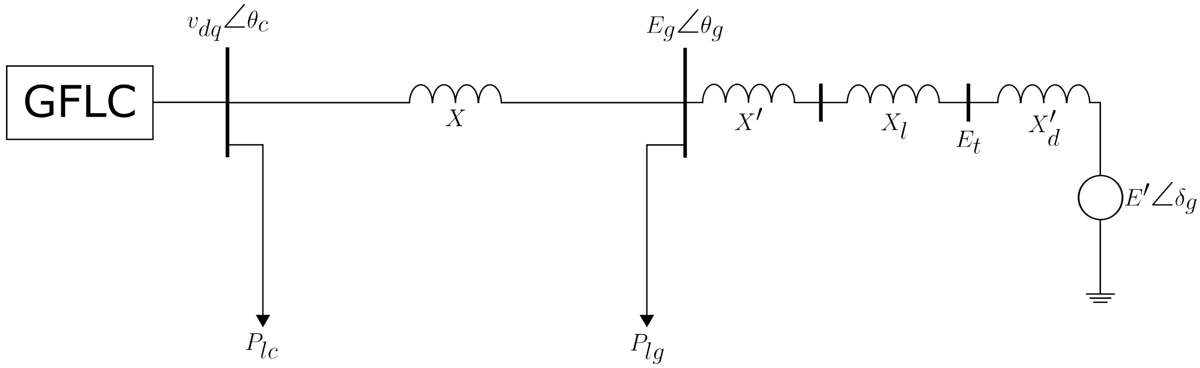

Figure 2.9. Power system represented by classical model of SG.

2.4.1 Phasor representation

Three different frames of references for the power system in figure 2.8 are shown in Fig. 2.10. The $R-I$ reference frame acts as the common frame of reference for both GFLC and SG. The vectors with respect to other two reference frames are projected on the common frame of reference to maintain the consistency while forming power flow equations which are described in next section.

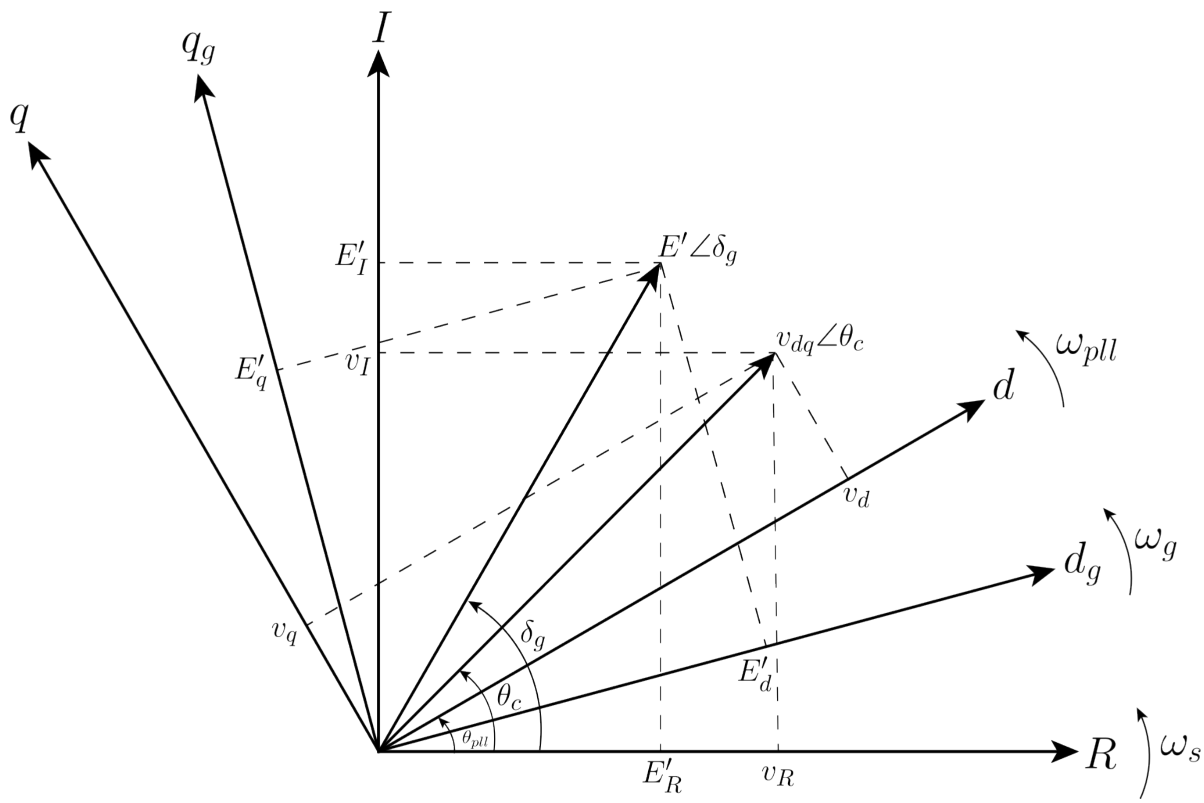

Figure 2.10. Phasor diagram.

2.4.2 Power flow equations of the network

The real and reactive power balance equations at GFLC bus are given by:

$$(v_{dq}\cos(\theta_c - \theta_{pll})i_d + v_{dq}\sin(\theta_c - \theta_{pll})i_q) = \frac{v_{dq}E_g}{X}(\sin(\theta_c - \theta_g)) + P_{lc} \tag{2.16}$$

$$(v_{dq}\sin(\theta_c - \theta_{pll})i_d - v_{dq}\cos(\theta_c - \theta_{pll})i_q) = \frac{v_{dq}^2}{X} - \frac{v_{dq}E_g}{X}(\cos(\theta_c - \theta_g)) \tag{2.17}$$

Similarly, the real and reactive power balance equations at SG bus are:

$$\frac{v_{dq}E_g}{X}(\sin(\theta_c - \theta_g)) + \frac{E'E_g}{X_l + X_d'}(\sin(\delta_g - \theta_g)) = P_{lg} \tag{2.18}$$

$$\frac{E_g^2}{X} - \frac{v_{dq}E_g}{X}(\cos(\theta_c - \theta_g)) + \frac{E_g^2}{X_l + X_d'} - \frac{E'E_g}{X_l + X_d'}(\cos(\delta_g - \theta_g)) = 0 \tag{2.19}$$

2.5 Formation of DAEs for the test system

The ODEs presented in sections 2.2 and 2.3, and the algebraic equations represented in section 2.4 are combined together to form the set of DAEs. In this system, there are a total of 10 differential and 4 algebraic equations, which are of the form $\dot{x} = f(x, z, u), 0 = g(x, z, u)$, where $x = \begin{bmatrix} i_d^* & i_d & x & v_{dqs} & i_q & \theta_{pll} & x_{pll} & \delta_g & \omega_g & P_m \end{bmatrix}^T \in \mathbb{R}^{10}$ are state variables, $z = \begin{bmatrix} \theta_c & v_{dq} & \theta_g & E_g \end{bmatrix}^T \in \mathbb{R}^4$ are the algebraic variables, and $u = \begin{bmatrix} i_q^* & E' & P_{lc} & P_{lg} \end{bmatrix}^T \in \mathbb{R}^4$ are the input variables. The nomenclature for each variables is described in previous sections during modeling, along with network diagram shown in figure 2.9.

2.6 Numerical solution of DAEs: state-of-art

In this section, state-of-art on the simultaneous approach is presented with the implicit integration method, Trapezoidal Method (TM). The DAEs in a compact form can be represented by the following equations [11]

$$\dot{x} = f(x, V) \tag{2.20}$$

$$0 = I(x, V) - Y_N V \tag{2.21}$$

In these equations x is a state vector representing state of individual devices, such that $x \in \mathbb{R}^n$, and $V \in \mathbb{R}^m$ represents the vector comprising real and imaginary parts of the bus voltages, $I \in \mathbb{R}^m$ is the vector consisting real and imaginary parts of current injections at each bus, and $Y_N \in \mathbb{R}^{m\times m}$ denotes the admittance matrix of the network in real form [11].

TM is a popular implicit numerical integration method used to solve DAEs. Discretization of (2.20) using TM provides the following expression [11]

$$F(x_{n+1}, V_{n+1}) = x_{n+1} - x_n - \frac{\Delta t}{2}(f(x_{n+1}, V_{n+1}) + f(x_n, V_n)) \tag{2.22}$$

In this equation F is known as the mismatch function for differential equations. It depends on the values of state variables at time instant t_n and t_{n+1}, values of functions as represented by (2.20) at t_n and t_{n+1}, and step-size Δt. Likewise, there is also a mismatch function for the algebraic equations presented in (2.21), which is defined as follows [11]

$$G(x_{n+1}, V_{n+1}) = Y_N V_{n+1} - I(x_{n+1}, V_{n+1}) \tag{2.23}$$

where, x_{n+1} and V_{n+1} can be found with the help mismatch functions by simultaneously solving the set of nonlinear algebraic equations as shown below

$$F(x_{n+1}, V_{n+1}) = 0, G(x_{n+1}, V_{n+1}) = 0 \tag{2.24}$$

Typically, for solving these equations, Newton's method is implemented [12]. The $(k+1)^{th}$ iteration of Newton's method can be obtained by following steps [11]:

$$\begin{bmatrix} x_{n+1}^{k+1} \\ V_{n+1}^{k+1} \end{bmatrix} = \begin{bmatrix} x_{n+1}^{k} \\ V_{n+1}^{k} \end{bmatrix} + \begin{bmatrix} \Delta x_{n+1}^{k} \\ \Delta V_{n+1}^{k} \end{bmatrix} \tag{2.25}$$

$$\begin{bmatrix} -F(x_{n+1}^{k}, V_{n+1}^{k}) \\ -G(x_{n+1}^{k}, V_{n+1}^{k}) \end{bmatrix} = \begin{bmatrix} \frac{\partial F}{\partial x_{n+1}} & \frac{\partial F}{\partial V_{n+1}} \\ \frac{\partial G}{\partial x_{n+1}} & \frac{\partial G}{\partial V_{n+1}} \end{bmatrix}_{n+1}^{k} \begin{bmatrix} \Delta x_{n+1}^{k} \\ \Delta V_{n+1}^{k} \end{bmatrix} \tag{2.26}$$

$$\begin{bmatrix} J \end{bmatrix} = \begin{bmatrix} \frac{\partial F}{\partial x_{n+1}} & \frac{\partial F}{\partial V_{n+1}} \\ \frac{\partial G}{\partial x_{n+1}} & \frac{\partial G}{\partial V_{n+1}} \end{bmatrix}_{n+1}^{k} = \begin{bmatrix} J_{11} & J_{12} \\ J_{21} & J_{22} \end{bmatrix} \tag{2.27}$$

In the above equations, J is the Jacobian matrix. At first, mismatch are calculated for both differential as well as algebraic equations using (2.22) and (2.23). After getting Jacobian matrix J from (2.27), Δx and ΔV are calculated with the help of (2.26). Then, the calculated values of Δx and ΔV are added to values of x and V of previous iteration to get the updated values of x and V, as shown in (2.25). The convergence criteria for newton iterations is $\| \begin{bmatrix} F^T & G^T \end{bmatrix}^T \|_\infty \leq \varepsilon$, where $\varepsilon \in \mathbb{R}_+$ is the tolerance of convergence.

TM can also be applied with varying step-size in order to obtain the results faster, but the step-size is typically not as large as Backward-Euler Method (BEM), which is to be discussed in chapter 4. The adaptive step-size control in TM is based on the local truncation error (LTE) method [21]. It basically speeds up the simulation with large step-sizes when the response of the system is not varying rapidly. While applying varying step-size with LTE in TM algorithm, there are certain steps which are needed to be rejected for reliable operation of TM, which can be done by having a minimum value and a maximum value of step-size that can selected by trial-and-error depending on the system characteristics. This means that the step-size is always bounded between a minimum and a maximum value when varying it based on LTE.

2.7 Summary

This chapter focuses on dynamic modeling of the power system. In this chapter, different control loops for the efficient operation of GFLC are described. Further, a power network is considered that includes a GFLC and a SG, where the SG is represented by its classical model. Then, DAEs in the form state-space equations of the GFLC and the SG, and real and reactive power flow of the network are used to represent the dynamic model of the system. Finally, the state-of-art in obtaining the solution for the DAEs involving TM is described.

The content of this chapter provides adequate background for the long-term simulation of power systems with IBRs to be presented in chapter 3.

Chapter 3 Long-term simulations of power systems with IBRs

3.1 Introduction

Chapter 2 described the modeling of DAEs in a power system with GFLCs and SGs. It also presented a numerical method called TM for solving DAEs, which a popular implicit numerical integration method. In TM, we need to restrict the step-size of the numerical integration. Therefore, for a large power system, it takes significant time for simulation. In this chapter, we will be discussing a numerical integration technique for solving the DAEs, which allows a large step-size, thereby providing a fast simulation process. Backward-Euler method (BEM) is the numerical integration method, which enable much faster simulations by neglecting oscillations and providing an approximate solution. This method basically focuses on extracting the end results from a system of DAEs rather than capturing their transient behavior.

3.2 Backward-Euler Method

BEM relies on Taylor series expansion centred at t_{n+1}, and then neglecting second and higher-order terms [12]. Discretization of (2.20) using BEM provides the following expression of mismatch function for differential equations [11]

$$F(x_{n+1}, V_{n+1}) = x_{n+1} - x_n - \Delta t(f(x_{n+1}, V_{n+1})) \tag{3.1}$$

The approach for solving DAEs using BEM is the same as that of TM as described in section 2.6, except the fact that mismatch function for differential equations is changed by (4.1).

The advantage of BEM is that we can have large step-sizes leading to fast simulation. A technique has been proposed in [22], for step-size control in BEM. The expression for varying the step-size is given by

$$\Delta t_{n+1} = \Delta t_n \frac{\tau}{\|b_x^0\|_\infty}, \ \Delta t_{min} \leq \Delta t_k \leq \Delta t_{max} \tag{3.2}$$

where, Δt_{min} and Δt_{max} are the parameters determined by the system and simulation speed versus accuracy tradeoff. The hyperparameter τ depends on the system conditions. It is to be tuned with trial-and-error adjustments to get appropriate results. $\|b_x^0\|_\infty$ is the largest magnitude of the first mismatch vector, which can be obtained by the following expression

$$\|b_x^0\|_\infty = \left\| \begin{bmatrix} F_x^0 \\ G_x^0 \end{bmatrix} \right\|_\infty \tag{3.3}$$

According to (4.2), the step-size is adjusted by the first mismatch vector. When $\frac{\tau}{\|b_x^0\|_\infty}$ is comparatively large, the step-size increases to approximate the response of the system.

While using varying step-size in BEM, their is a upper limit that have to be placed on the next step-size i.e Δt_{n+1}. As the system response converges to its final value, the first mismatch vector becomes negligible, thereby $\|b_x^0\|_\infty$ also becomes negligible and according to (4.2), Δt_{n+1} becomes significantly large. Hence, a maximum step-size limit is required, which can vary depending on the system. The maximum step-size can be chosen by trial-and-error for reliable operation of the algorithm.

3.3 Study system

The single line diagram of the test system under consideration is shown in Fig. 3.1. All of the parameters of the system are expressed in per-unit (pu), with a 100 MVA base. The voltage base for GFLC, transmission line and SG are 480V, 230 kV and 20 kV, respectively. The power rating of GFLC is 6 pu and it is delivering 4.5 pu of real power, whereas SG is rated at 9 pu and is delivering 7 pu real power to the network under nominal condition. There are two real power loads, one of which is connected to the GFLC bus (P_{lc}) and other is connected the SG bus (P_{lg}). Under nominal conditions, the GFLC delivers half of its power to P_{lc}, i.e., 2.25 pu and the other half is being provided to P_{lg} through transmission line, which is considered lossless. On the other hand, the

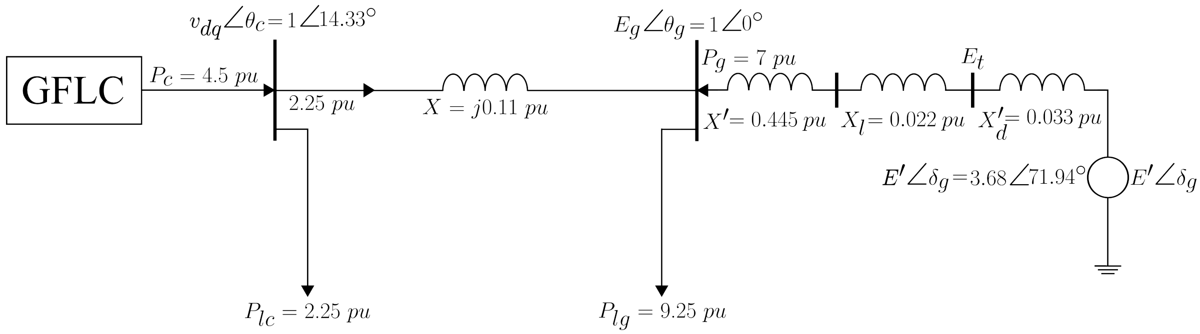

Figure 3.1. Single line diagram of the study system.

SG is delivering its entire power to load P_{lg}. Therefore, the total load consumed by P_{lg} is 9.25 pu. The magnitude $v_{dq} = E_g = 1\ pu$ and the angle θ_g is assumed to be 0°. The angle θ_c can be calculated by the real power transfer equation through transmission line. It is assumed that vector $v_{dq}\angle\theta_c$ is aligned to d-axis of $d - q$ rotating frame of PLL, thus initially $\theta_{pll} = \theta_c$. Calculations are performed to get magnitude and angle of voltage behind transient reactance of the SG model. The GFLC is also supplying reactive power to the system to maintain 1 pu voltage at the GFLC bus. The control gains K_p and K_i for the outer voltage control loop are 5 and $0.5s^{-1}$, respectively. On the other hand, The control gains K_p^{pll} and K_i^{pll} for the PLL are 101 $rad - s^{-1}pu^{-1}$ and 2562 $rad - s^{-2}pu^{-1}$, respectively. The values of d_{pg}, R_{pc} and K_{ip} are $\frac{1}{2\pi}\ pu\, rad^{-1} - s$, $2\pi\ pu\, rad^{-1} - s$ and 141.6 pu^{-1}, respectively. The time-constants for governer (τ_g), voltage (τ_v) and current (τ_i) are $5s$, $0.05s$ and $\frac{1}{300}s$, respectively. The inertia constant H_g of the SG is $58.5s$.

3.4 Simulation results

At $1s$, a step change of 0.5 pu is provided to the load P_{lc}, such that it consumes 2.75 pu of real power. The simulation is run for $30s$ and results are observed. Although the simulations are run for $30s$, the sustainability of the proposed approach using BEM for long-term simulations will be apparent when results are analysed. The simulation is performed for two test cases, (i) with nominal length ($X = 0.11\ pu$) and (ii) double the length ($X = 0.22\ pu$) of transmission line with three different numerical integration methods, namely

(1) TM with fixed step-size of 1 ms
(2) TM with variable step-size
(3) BEM with variable step-size

The results of the simulations are as follows:-

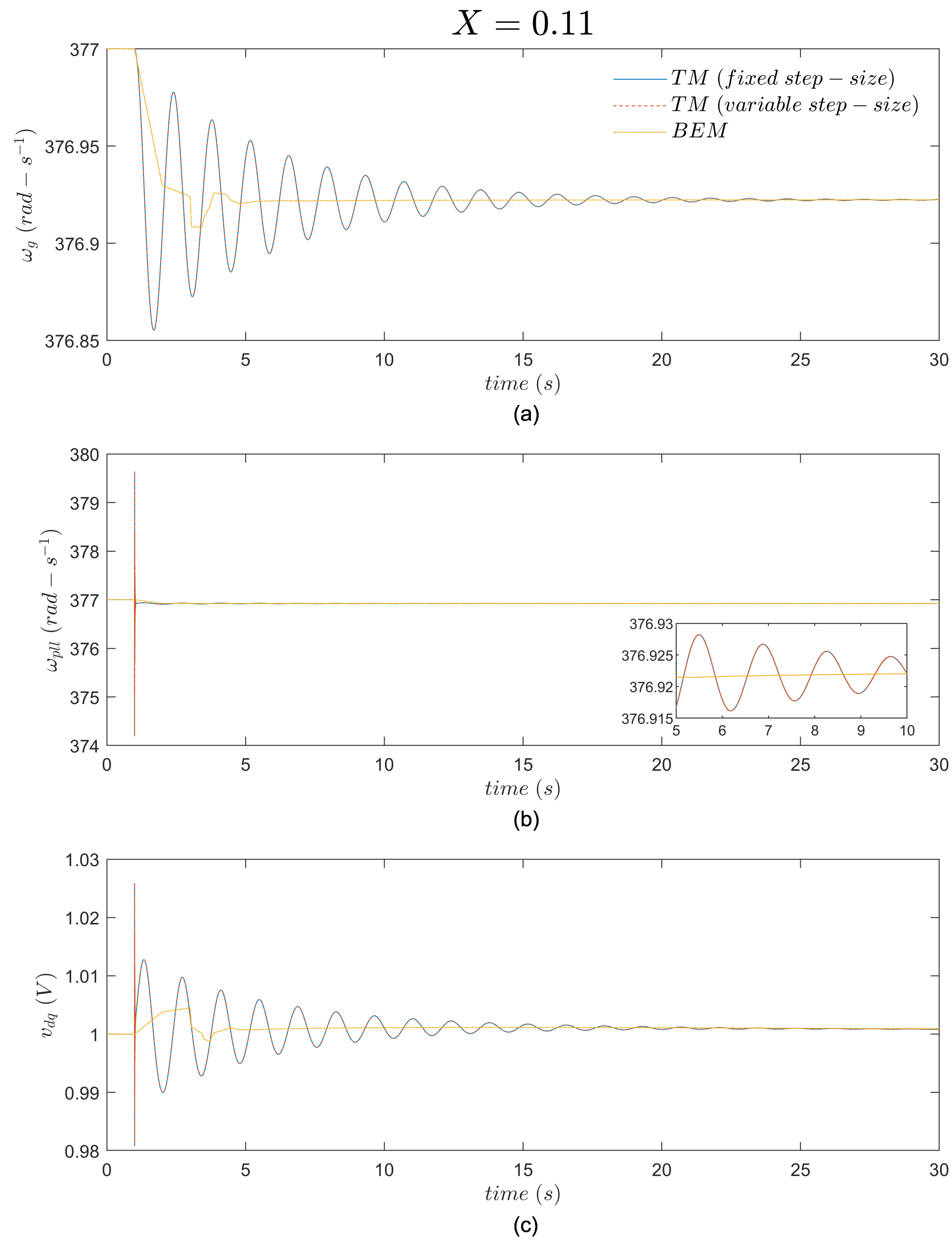

Figure 3.2. Simulation results (a) rotor speed (b) angular frequency of PLL (c) voltage at GFLC bus.

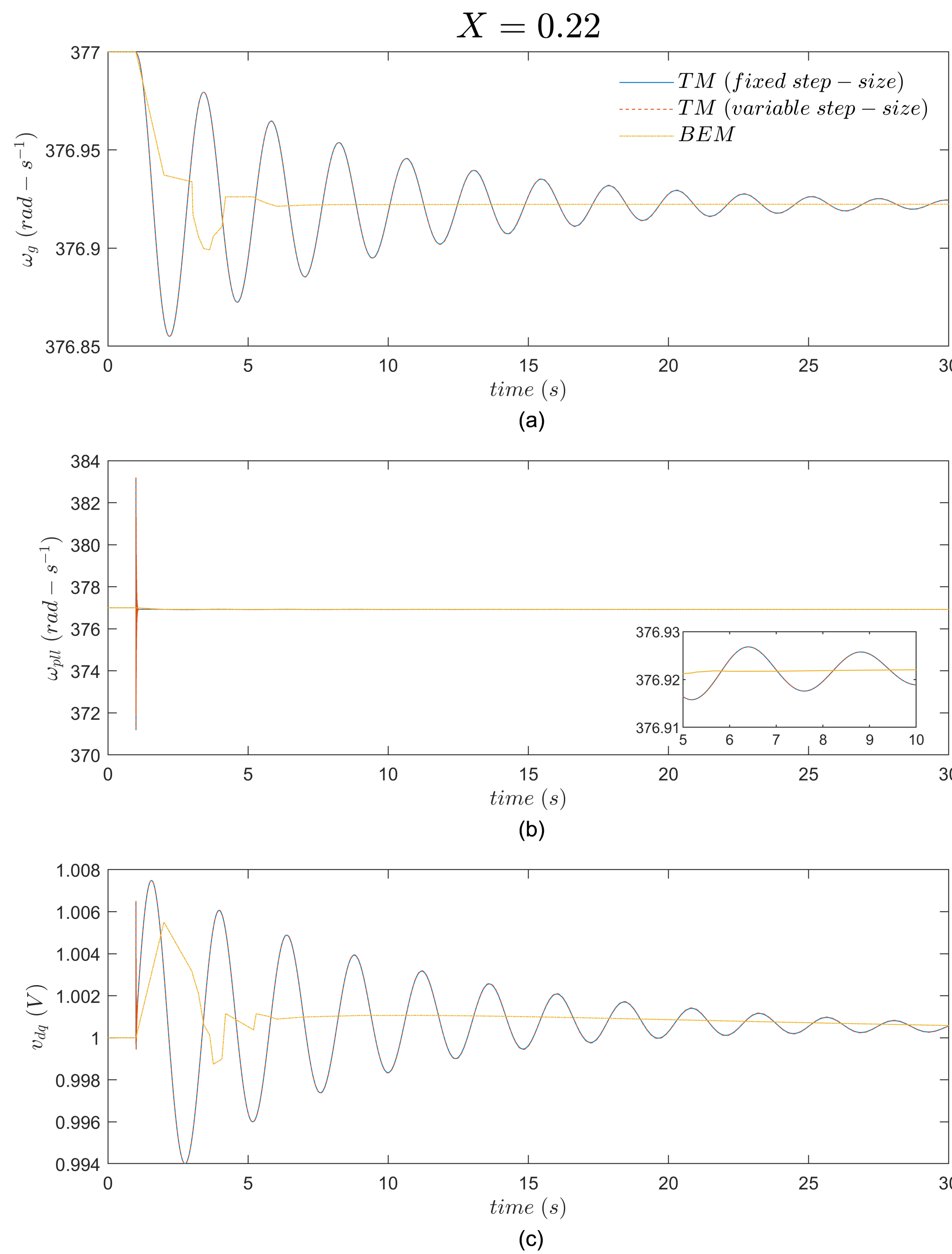

Figure 3.3. Simulation results (a) rotor speed (b) angular frequency of PLL (c) voltage at GFLC bus.

As per Fig. 3.2 and Fig. 3.3, it can been seen that BEM is successfully providing the approximate response of the system by neglecting oscillations, which are observed with the TM algorithm. TM with adaptive step-size control based on LTE method is perfectly overlapping to the oscillation as that of TM with fixed step-size.

Table 3.1 shows the time taken by each numerical method for both nominal and double the length of line. BEM provides results at least simulation time, proving that it is an efficient approach for long-term simulations of power systems, followed by TM with variable step-size. TM with fixed step-size has the largest simulation time as shown by table 3.1.

Simulation time (in s)			
	TM (fixed time-step)	TM (variable time-step)	BEM
$X = 0.11$	2.82	2.16	1.29
$X = 0.22$	2.99	2.23	1.32

Table 3.1. Simulation time with different numerical integration methods

Solving DAEs with BEM can also lead to unstable equilibrium point due to a property known as hyperstability. The oscillatory instability can be detected by eigendecomposition of system matrix (A matrix) around this equilibrium as mentioned in [11].

3.5 Summary

In this chapter, we described the long-term simulation process for power system with the help of BEM algorithm. The test system for simulation was described, along with the initial values at nominal state. The simulation was performed for three different numerical integration techniques and results were presents for two test cases. The simulation results show that simulation time with BEM is comparatively less than that of TM. Therefore, BEM can be successfully implemented for long-term simulations of power systems with IBRs. Also, TM with variable step-size based LTE can be applied to observe the ground truth of the simulations with reduced simulation time.

Chapter 4 Protection of power systems with IBRs

4.1 Introduction

In previous chapter, we discussed a proposed approach for long-term simulations of power systems with dynamic models of GFLC and SG. In this chapter, we will be investigating the impact of IBRs on performance of a distance relay designed for the protection of conventional power system. The distance relay is used to protect transmission line by measuring the impedance as viewed from relay location. The simulation of the relay is performed in MATLAB/Simulink and the results are presented in this chapter.

4.2 Distance protection

In high-voltage overhead transmission lines, the most common protection scheme used is distance protection. There are different types of distance protection relays used for power system protection such as impedance relays, reactance relays and mho relays. The distance protection is generally more selective and offers faster criteria to isolate the fault from the system as compared to overcurrent protection as it identifies the fault location quickly. Also, distance protection is a robust and reliable type of protection due to its less susceptibility to changes in system conditions [23].

The basic principle of distance protection is to measure the voltage to current ratio or impedance of the line as viewed from relay location. It operates when the measured impedance of the line falls below predetermined threshold impedance, which indicates the fault in the transmission line and trips the section of line with fault, whereas other parts of the system remain intact [24].

4.3 Operational challenges in distance protection with IBRs

Short-circuit fault current is impacted by presence of IBRs in the system, thus the voltage to current ratio is also affected. This may cause false-tripping of the transmission lines during normal operation as well as fault conditions [25].

Moreover, the negative sequence current component of the fault current are insufficient, which may result in mis-operation of directional relays [26]. IEEE P2800 [27] signifies the need to produce negative sequence current by IBRs. Lack of negative sequence current in the system poses a functional difficulty to relays in determining the directionality of protective elements, hence leading to undesired operations or mis-operation in case of faults [28].

4.4 Relay design

The protection system developed uses distance relaying principle, specifically implementing impedance relays. The impedance relay characteristics on the R-X diagram is shown in Fig. 4.1 [24].

As represented in Fig. 4.1, the impedance relay operates in all four quadrants of R-X plane, which means it is independent of phase relation between voltage and current, thus directionally independent. The boundary of R-X diagram in impedance relay characteristics represents the magnitude of impedance of transmission line up to which relay is designed to protect. Under normal conditions, the impedance or voltage to current ratio (V/I) as viewed from the relay location remains outside the R-X diagram, but under the influence of short-circuit fault in the transmission line, the voltage decreases and current increases, hence ratio V/I decreases. When the ratio V/I lies inside the R-X characteristic, the relay trips representing that a fault has occurred within the reach of relay.

The block diagram in Fig. 4.2 represents the typical operation of relay in presence of grid-following IBRs. A delay of one-cycle (16.7 ms for this model) is provided to avoid mis-tripping of the relay. The delay is implemented to prevent the tripping of the relay is case of self-clearing faults.

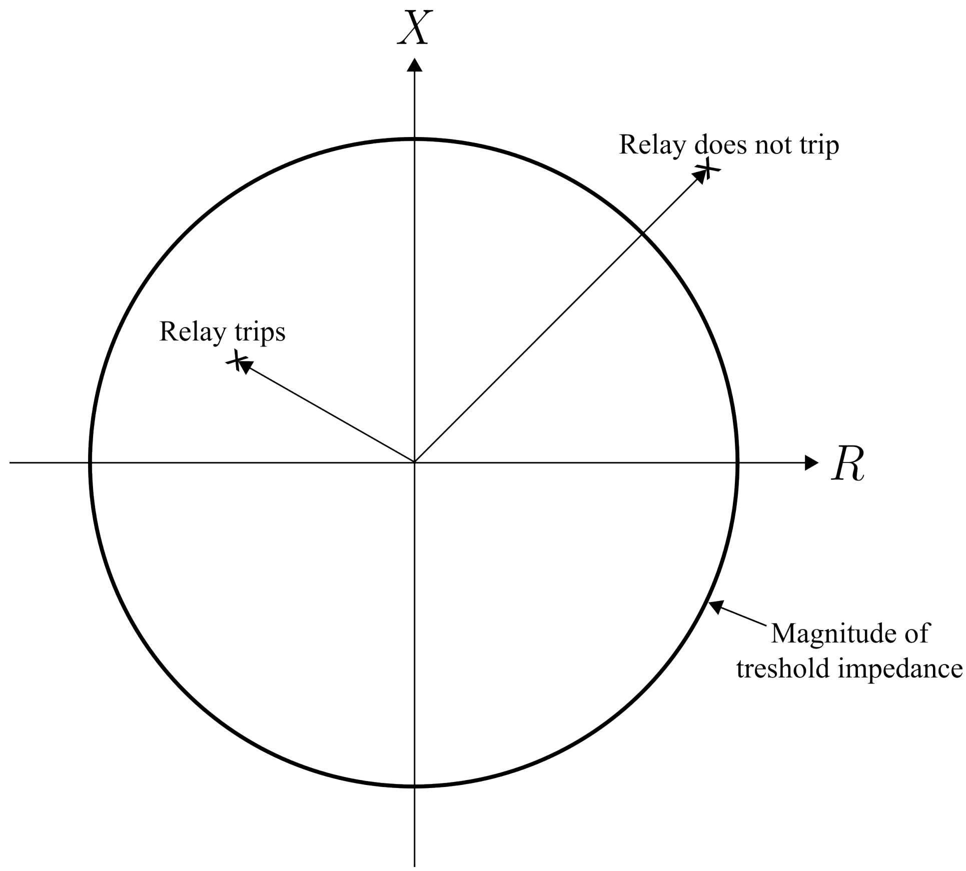

Figure 4.1. R-X characteristic diagram of impedance relay.

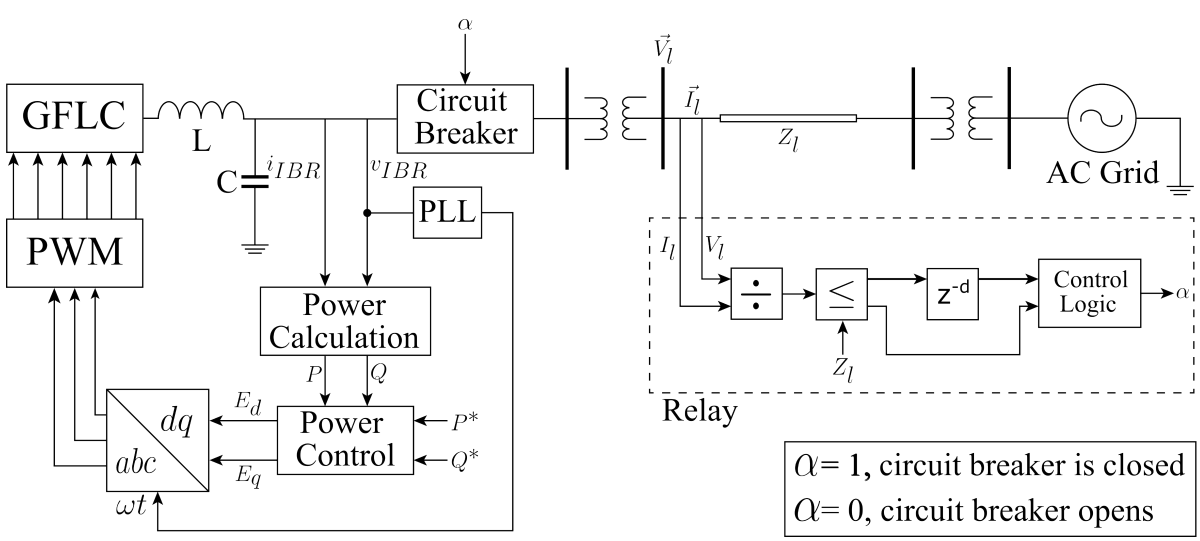

Figure 4.2. Model of a distance relay connected to the power system with GFLC. Relay parameters were originally designed for a system where SG was present in place of GFLC.

A control logic is used which compares the delayed output to that of original trip signal. With the help of the control logic, the relay only trips for the faults when the impedance during short-circuit faults lies inside the R-X characteristics for more than one-cycle. It has to be noted that the relay shown in Fig. 4.2 is primarily designed for protection of conventional power system, and then its behavior in presence of IBRs is observed. The AC grid in Fig. 4.2 is represented by an ideal voltage behind series impedance.

In the relay model in Fig. 4.2, Z_l represents the impedance of the transmission line within reach of relay, whereas V_l and I_l represents the voltage and current magnitudes, respectively at the relay location. The input to the circuit breaker is α and it is initially closed when $\alpha = 1$. Whenever, the fault occurs within the reach of the relay, the control logic gives an output $\alpha = 0$, which is referred as the trip signal by the relay. With trip signal $\alpha = 0$, circuit breakers open and isolate the transmission line from the system.

4.5 Simulation set-up

The relay was tested separately with SG and Photovoltaic (PV) as the IBR, integrated to the AC grid for synchronization. Detailed modeling of PV-IBR (grid-following mode) is explained in [3]. The terminal voltage of the SG is 13.8 kV rms (phase-to-phase) with nominal power of 187 MVA. The PV is providing an output DC voltage of 500 V. A three-phase DC/AC inverter is used to convert DC to AC. The terminal voltage of the inverter is 250 V rms (phase-to-phase). The system frequency is 60 Hz. The transmission line considered is 200 km long at 69 kV voltage for each test case. Transformers with voltage rating of 13.8/69 kV and 0.25/69 kV are used to step-up the voltage for the transmission system in case of SG and IBR, respectively. The relay is designed to protect 100 Km of the transmission line. A three-phase fault occurs at the transmission line at 0.2 s and results are observed.

4.6 Simulation results

The simulations are performed for two different test systems, namely with SG and IBR, with three-phase fault at 90 Km, 120 Km and 125 Km of transmission line from the SG/IBR.

The results of the simulations are as follows:-

(i) SG:

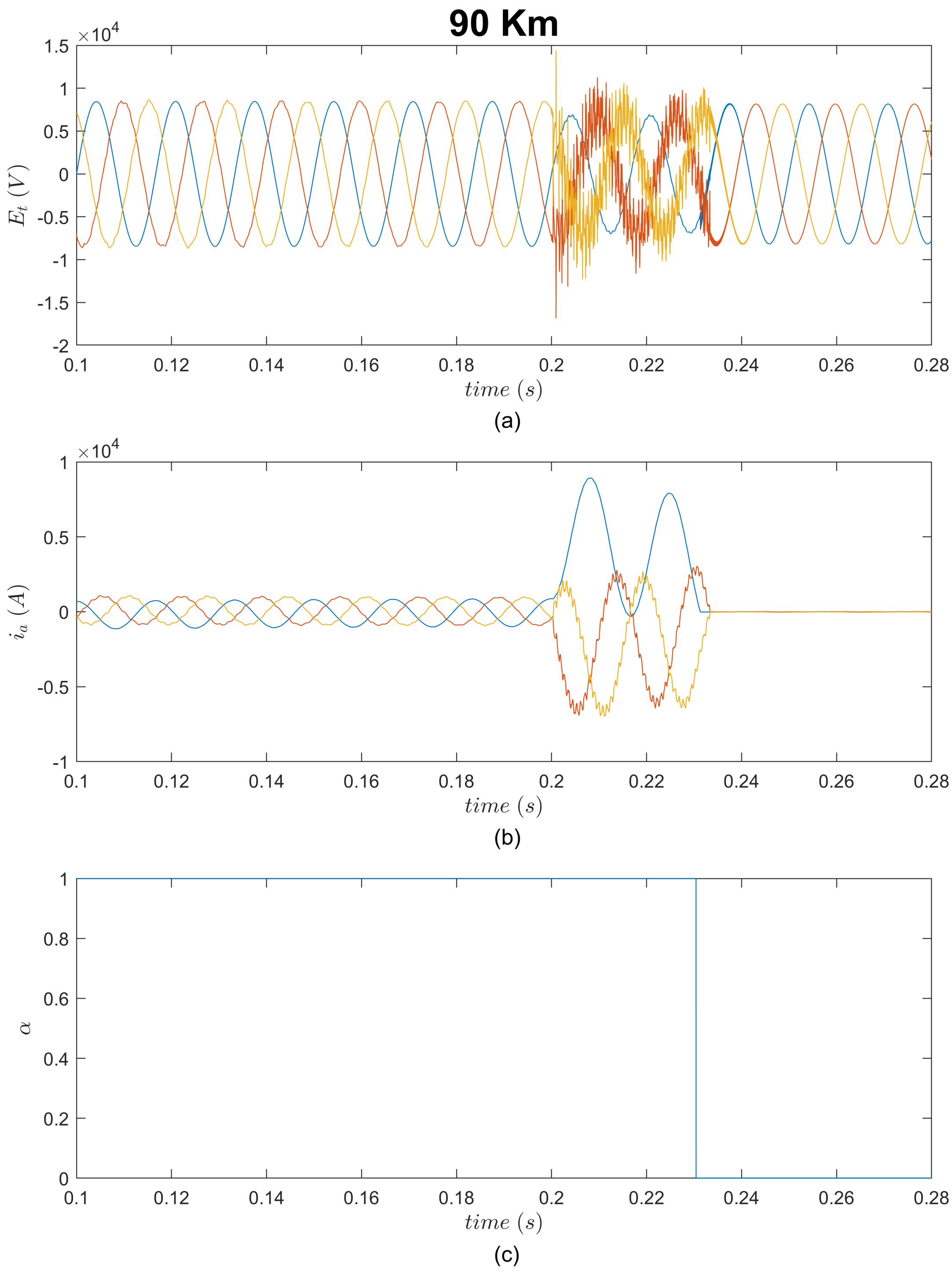

Figure 4.3. Simulation results for fault at 90 Km of transmission line (a) terminal voltage SG (b) stator current (c) trip signal.

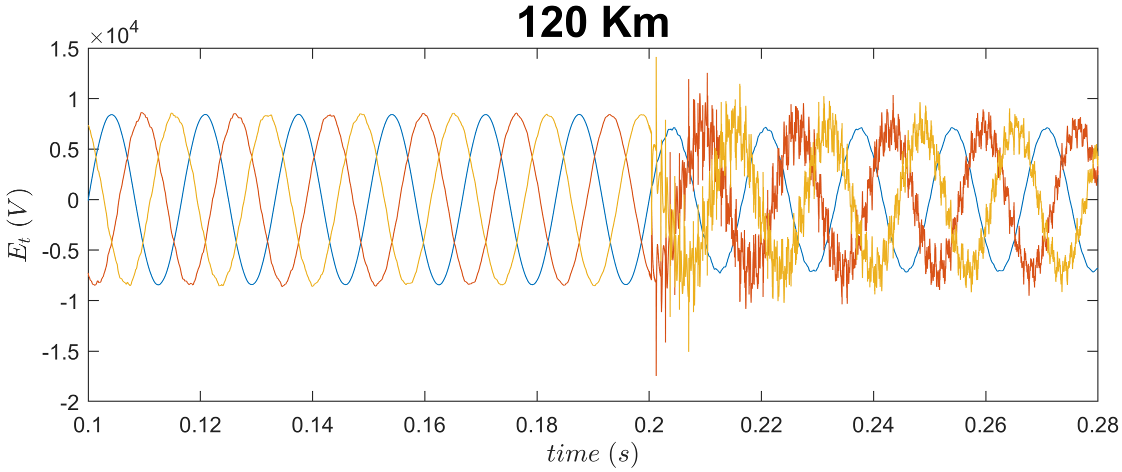

(a)

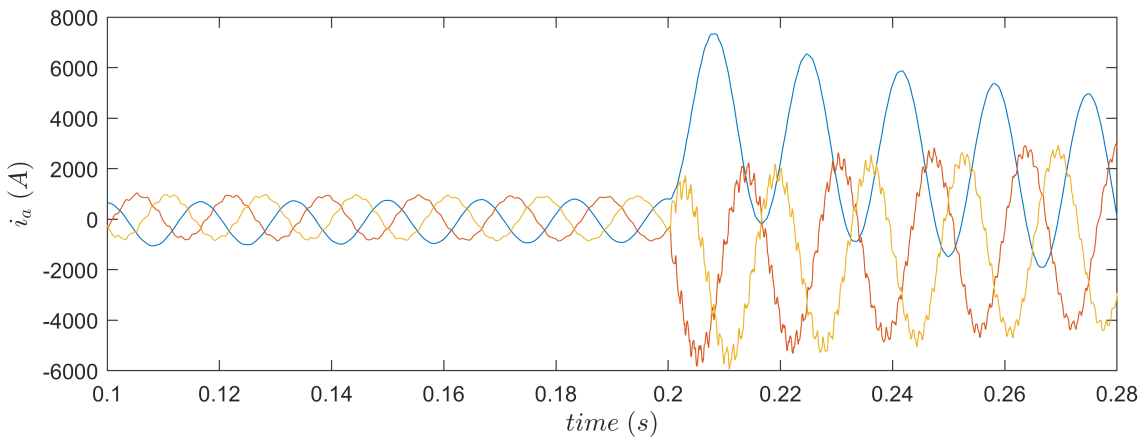

(b)

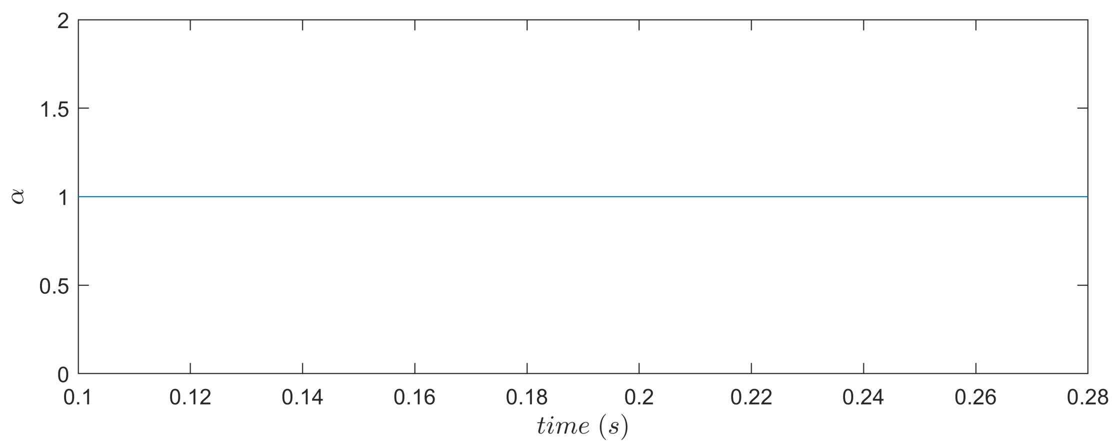

(c)

Figure 4.4. Simulation results for fault at 120 Km of transmission line (a) terminal voltage SG (b) stator current (c) trip signal.

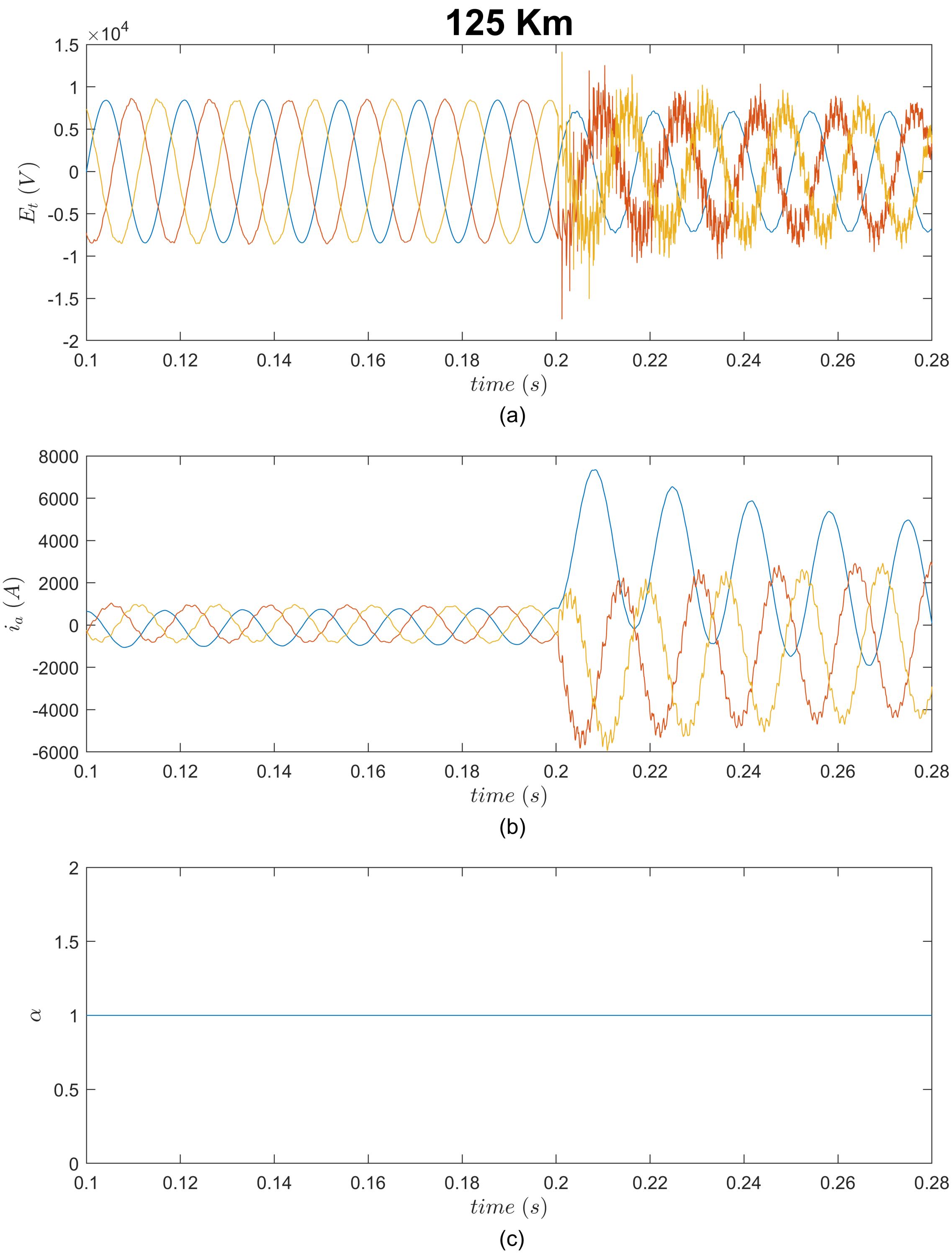

Figure 4.5. Simulation results for fault at 125 Km of transmission line (a) terminal voltage SG (b) stator current (c) trip signal.

(*ii*) IBR:

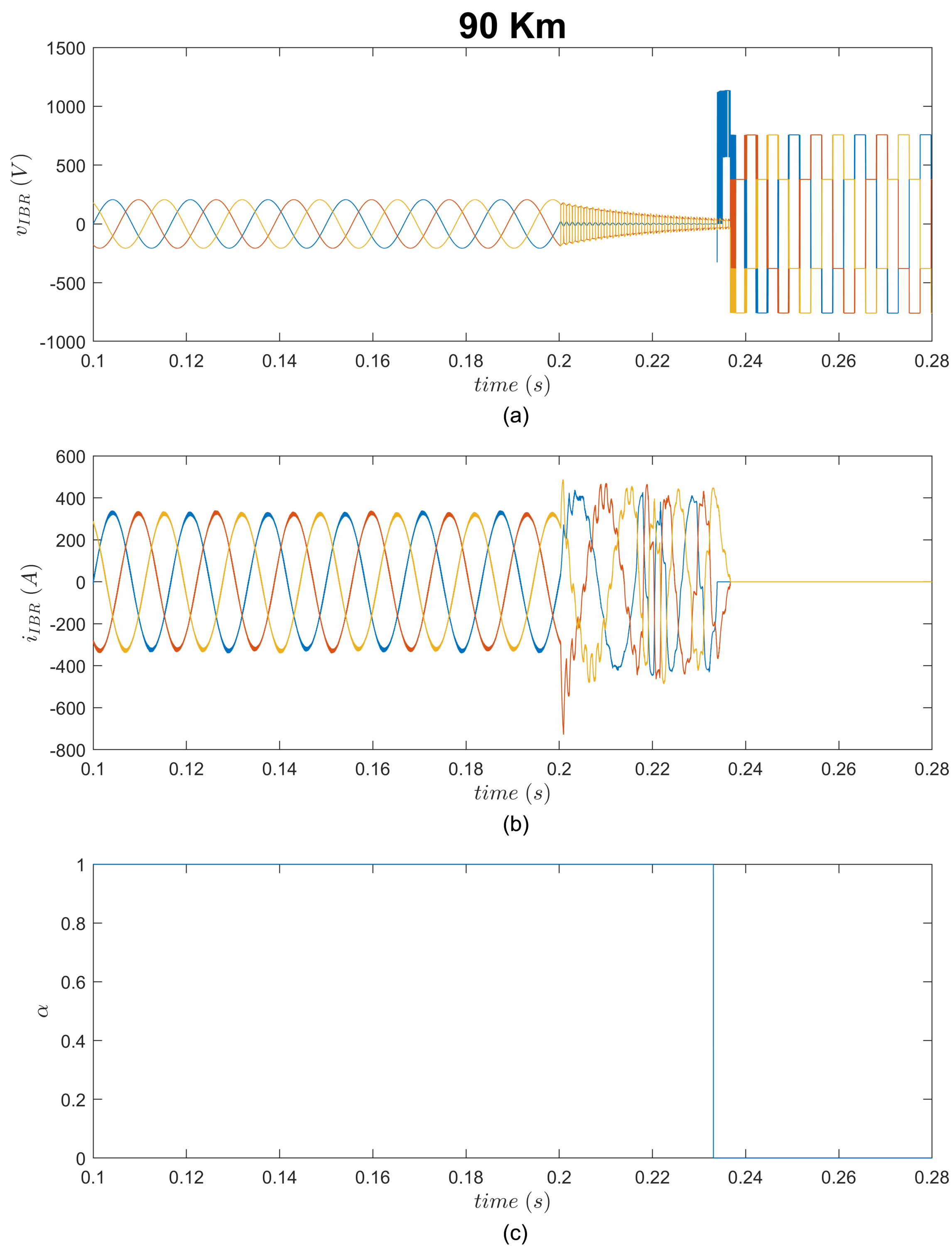

Figure 4.6. Simulation results for fault at 90 Km of transmission line (a) terminal voltage of inverter (b) IBR current (c) trip signal.

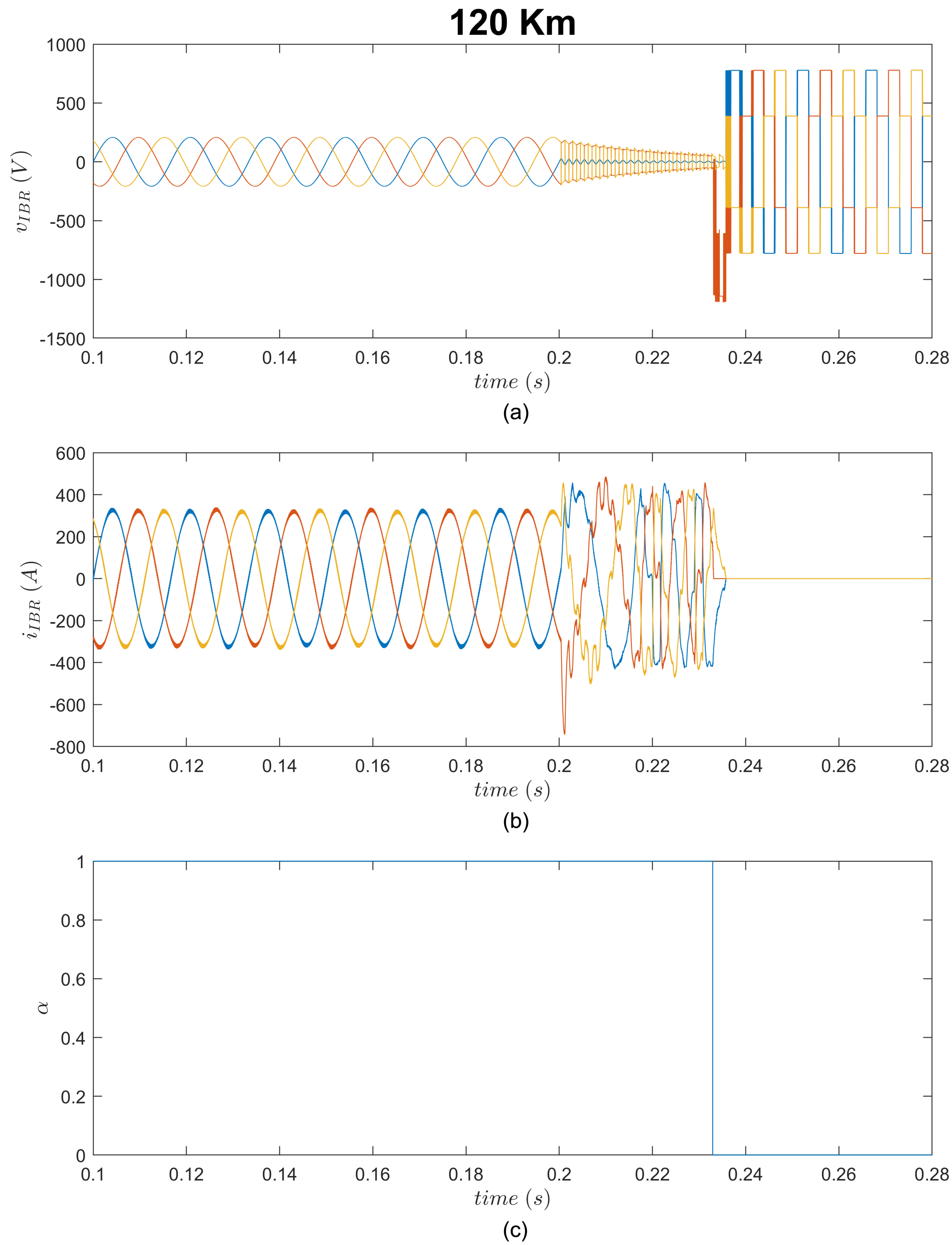

Figure 4.7. Simulation results for fault at 120 Km of transmission line (a) terminal voltage of inverter (b) IBR current (c) trip signal.

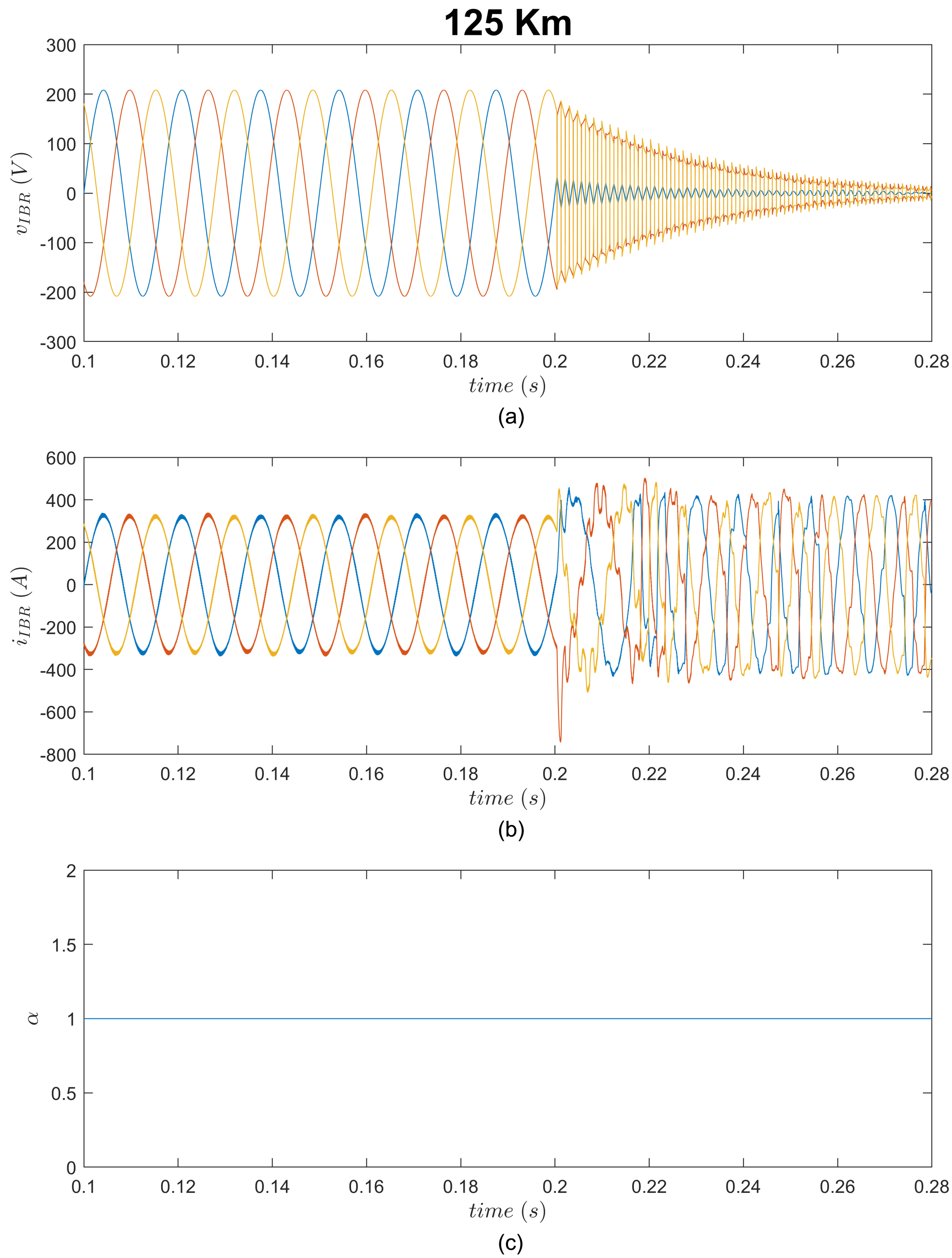

Figure 4.8. Simulation results for fault at 125 Km of transmission line (a) terminal voltage of inverter (b) IBR current (c) trip signal.

The results show that for fault occurring at 90 Km of the transmission line, the relay trips for both the cases and sends a signal (Fig. 4.3(c) and Fig. 4.6 (c)) to circuit breaker to open. Figures 4.3 (a) and 4.3 (b) shows the terminal voltage and stator current of SG, whereas Fig. 4.6 (a) and Fig. 4.6 (b) shows the voltage and current waveforms from IBR.

Simulation results of Fig. 4.7 shows that for the fault occurring at 120 Km of transmission line, relay trips in connection to IBR, whereas it does not trip when connected to SG (Fig. 4.4). This shows that the relay is tripping only for fault inside the reach with SG, but shows an overreach of 120% as it also trips for fault beyond its reach when connected to IBR.

For the fault occurring at 125 Km of transmission line, relay does not trip for both test systems as represented by Fig. 4.5 and Fig. 4.8, showing its efficient operation for faults beyond 120% of its range when connected to IBR.

The comparison of Figs. 4.3(b)-4.5(b) and Figs. 4.6(b)-4.8(b) show the difference between short-circuit contribution of SG versus IBR. While the SG current contribution is significant, the IBR current contribution is restricted because of its current limiting features.

4.7 Summary

The designed impedance relay protects the transmission line during the fault by isolating the faulted section of transmission line with the help of circuit breaker. During fault, relay trips and send a signal to circuit breakers to open. As designed, the relay shows an efficient operation in conventional power system. However, it shows an overreach of 120% when SG is replaced by IBR as it also trips for faults beyond its range. Further research should be performed in this area to avoid such mis-operations.

Chapter 5 Conclusion and future work

5.1 Conclusion

Long-term simulation of IBRs in power system in case of disturbance is discussed, along with development of protection scheme to protect the IBRs from short-circuit faults. Simulations results show that Backward-Euler Method (BEM) successfully approximates the trajectories of dynamic model of power system obtained from Trapezoidal Method (TM) and provides the equilibrium much faster. Variable step-size used in TM provides the similar response of the system to that obtained from constant step-size but in less period, hence proving its reliability in getting the results faster, while observing the ground truth of the dynamic model of power systems.

The designed protection system is successfully isolating the transmission line in case of short-circuit fault. However, the relay is showing an overreach of 120% in protecting power systems with IBRs as it is also tripping for faults which tends to be outside its zone.

5.2 Future work

The protection system with IBRs and long-term simulation process has a lot of potential for the researchers to pursue their research in continuation to the work presented in this thesis. This work can act as a background for cascading failure analysis in IBR-dominated power grid. In cascading failure analysis, the goal is to obtain a new equilibrium in less time period for which long-term simulation process can be implemented. Also, the relay presented in this thesis can be used to trip faulted section of transmission line out of the system, whenever a fault occurs. After obtaining a new equilibrium and comparing it with the threshold, the relays will be able to decide whether to trip other components consecutively.

Appendix I
$dq0$ and inverse $dq0$ transformation

1 Introduction

This Appendix describes the transformation of abc reference frame to $dq0$ and its inverse. This transformation in widely used in GFLC technology, for conversion of three-phase voltage and current in abc reference frame to $dq0$ reference frame, for the operation of PLL. After obtaining a reference angle ωt from PLL, the inverse $dq0$ transformation is implemented to provide reference to each phase in abc frame. The detailed explanation of $dq0$ and inverse $dq0$ transformation can be obtained from [29].

2 $dq0$ transformation

The $dq0$ reference frame is a rotating frame for AC quantities such the AC signal appears to be DC for analysis. A three-phase AC voltage signal can be represented by:

$$v_a = V_m cos(\omega t + \alpha) \tag{1}$$

$$v_b = V_m cos(\omega t - 120^\circ + \alpha) \tag{2}$$

$$v_b = V_m cos(\omega t + 120^\circ + \alpha) \tag{3}$$

Where V_m is the peak value of the signal and α is the phase. v_a, v_b and v_c represents the voltage signal for each phase.

The $dq0$ transformation of AC signal is given by:

$$v_{dq0} = T_\theta v_{abc} \tag{4}$$

$v_{abc} = \begin{bmatrix} v_a & v_b & v_c \end{bmatrix}^T$ and $v_{dq0} = \begin{bmatrix} v_d & v_q & v_0 \end{bmatrix}^T$ represented the system matrix in *abc* and $dq0$ frame, respectively. T_θ is known as the transformation matrix which is equal to

$$T_\theta = \frac{2}{3} \begin{bmatrix} cos(\theta) & cos(\theta - 120^\circ) & cos(\theta + 120^\circ) \\ -sin(\theta) & -sin(\theta - 120^\circ) & -sin(\theta + 120^\circ) \\ \frac{1}{2} & \frac{1}{2} & \frac{1}{2} \end{bmatrix} \tag{5}$$

So, $dq0$ transformation in the matrix form is represented by:

$$\begin{bmatrix} v_d \\ v_q \\ v_0 \end{bmatrix} = \frac{2}{3} \begin{bmatrix} cos(\theta) & cos(\theta - 120^\circ) & cos(\theta + 120^\circ) \\ -sin(\theta) & -sin(\theta - 120^\circ) & -sin(\theta + 120^\circ) \\ \frac{1}{2} & \frac{1}{2} & \frac{1}{2} \end{bmatrix} \begin{bmatrix} v_a \\ v_b \\ v_c \end{bmatrix} \tag{6}$$

The angle θ in above equations is the angle difference between phase a of *abc* frame and $d-$axis of $dq0$ reference frame as shown by Fig. 1. The angle θ is varying with time as $dq0$ frame is rotating continuously. It has to be noted that the factor $\frac{2}{3}$ can vary depending upon the system [3]. However, for the scope of work presented in this thesis, we are taking the factor for $dq0$ transformation as 1.

3 Inverse $dq0$ transformation

Inverse $dq0$ transformation is referred as obtaining three-phase AC signal in *abc* frame from $dq0$ quantities which is defined as

$$v_{abc} = T_\theta^{-1} v_{dq0} \tag{7}$$

T_θ^{-1} is the inverse transformation matrix represented as:

$$T_\theta^{-1} = \begin{bmatrix} cos(\theta) & -sin(\theta) & 1 \\ cos(\theta - 120^\circ) & -sin(\theta - 120^\circ) & 1 \\ cos(\theta + 120^\circ) & -sin(\theta + 120^\circ) & 1 \end{bmatrix} \tag{8}$$

Inverse $dq0$ transformation in matrix form is given by

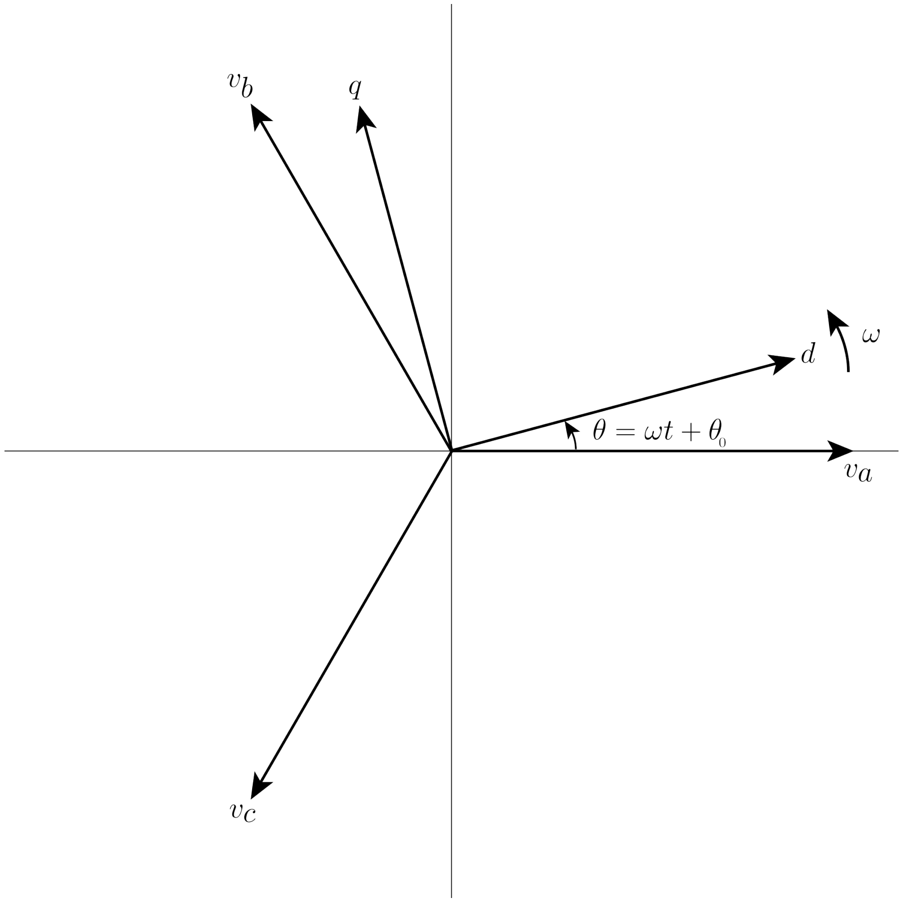

Figure 1. *dq*0 transformation [3].

$$\begin{bmatrix} v_a \\ v_b \\ v_c \end{bmatrix} = \begin{bmatrix} cos(\theta) & -sin(\theta) & 1 \\ cos(\theta - 120°) & -sin(\theta - 120°) & 1 \\ cos(\theta + 120°) & -sin(\theta + 120°) & 1 \end{bmatrix} \begin{bmatrix} v_d \\ v_q \\ v_0 \end{bmatrix} \tag{9}$$

Direct multiplication of the transformation and inverse transformation matrices results in identity matrix of order 3×3.

$$T_\theta T_\theta^{-1} = T_\theta^{-1} T_\theta = I_{3\times 3} \tag{10}$$

4 Real and reactive power calculation from voltage and current in $dq0$ reference frame

With the $dq0$ transformation factor as 1, as in the scope of work in this thesis, the current and voltage in $dq0$ reference frame can be presented as:

$$v = v_d + jv_q \tag{11}$$

$$i = i_d + ji_q \tag{12}$$

The complex power (S) of the network can be calculated by:

$$S = vi^* \tag{13}$$

where * represents the conjugate of complex number. Hence,

$$S = (v_d + jv_q)(i_d - ji_q) \tag{14}$$

The real and reactive power from the complex power can be obtained as:

$$P = Re\{S\} \tag{15}$$

$$Q = Im\{S\} \tag{16}$$

The real and reactive power from the parameters in $dq0$ frame can be represented as:

$$P = v_d i_d + v_q i_q \tag{17}$$

$$Q = v_q i_d - v_d i_q \tag{18}$$

Bibliography

[1] J. Machowski, Z. Lubosny, J. Bialek, and J. Bumby, *Power System Dynamics: Stability and Control*. Wiley, 2020.

[2] P. Kundur, "Power system stability and control," 1994.

[3] Y. Li, *Cyber-Physical Microgrids*. Springer International Publishing, 2021.

[4] U. S. E. P. Agency, "Sources of greenhouse gas emissions," 2021.

[5] U. E. I. Administration, "Electricity explained-basics," 2019.

[6] B.-M. S. Hodge, H. Jain, C. Brancucci, G.-S. Seo, M. Korpås, J. Kiviluoma, H. Holttinen, J. C. Smith, A. Orths, A. Estanqueiro, L. Söder, D. Flynn, T. K. Vrana, R. W. Kenyon, and B. Kroposki, "Addressing technical challenges in 100% variable inverter-based renewable energy power systems," *WIREs Energy and Environment*, vol. 9, no. 5, p. e376, 2020.

[7] F. Milano, F. Dorfler, G. Hug, D. Hill, and G. Verbič, "Foundations and challenges of low-inertia systems (invited paper)," in *2018 Power Systems Computation Conference (PSCC 2018)* (M. Paolone and C. Rehtanz, eds.), pp. 1 – 25, IEEE, Institute of Electrical and Electronics Engineers, 2018.

[8] F. Katiraei and J. R. Agüero, "Solar PV integration challenges," *IEEE Power and Energy Magazine*, vol. 9, no. 3, pp. 62–71, 2011.

[9] J. Jana, K. D. Bhattacharya, and H. Saha, "Trends and challenges of next generation grid connected photovoltaic inverter — an overview," *2017 Australasian Universities Power Engineering Conference (AUPEC)*, pp. 1–6, 2017.

[10] J. Bialek, T. Bowen, T. Green, D. Lew, Y. Li, J. MacDowell, J. Matevosyan, N. Miller, M. O'Malley, and D. Ramasubramanian, "System needs and services for systems with high ibr penetration," *Global PST Consortium*, 2021.

[11] S. Gharebaghi, N. R. Chaudhuri, T. He, and T. La Porta, "An approach for fast cascading failure simulation in dynamic models of power systems," *Applied Energy*, vol. 332, p. 120534, 2023.

[12] U. M. Ascher and L. R. Petzold, "Computer methods for ordinary differential equations and differential-algebraic equations," 1998.

[13] A. Haddadi, E. Farantatos, I. Kocar, and U. Karaagac, "Impact of inverter based resources on system protection," *Energies*, vol. 14, no. 4, p. 1050, 2021.

[14] H. Urdal, R. Ierna, J. Zhu, C. Ivanov, A. Dahresobh, and D. Rostom, "System strength considerations in a converter dominated power system," *IET Renewable Power Generation*, vol. 9, pp. 10–17, 2015.

[15] J. Keller and B. Kroposki, "Understanding fault characteristics of inverter-based distributed energy resources,"

[16] E. Muljadi, N. Samaan, V. Gevorgian, J. Li, and S. Pasupulati, "Different factors affecting short circuit behavior of a wind power plant," in *2010 IEEE Industry Applications Society Annual Meeting*, pp. 1–9, 2010.

[17] A. Yazdani and R. Iravani, "Voltage-sourced converters in power systems: Modeling, control, and applications," 2010.

[18] A. Tayyebi, D. Groß, A. Anta, F. Kupzog, and F. Dörfler, "Frequency stability of synchronous machines and grid-forming power converters," *IEEE Journal of Emerging and Selected Topics in Power Electronics*, vol. 8, no. 2, pp. 1004–1018, 2020.

[19] S.-K. Chung, "A phase tracking system for three phase utility interface inverters," *IEEE Transactions on Power Electronics*, vol. 15, no. 3, pp. 431–438, 2000.

[20] O. I. Elgerd and H. H. Happ, "Electric energy systems theory: An introduction," 1972.

[21] D. F. Griffiths and D. J. Higham, "Numerical methods for ordinary differential equations - initial value problems," in *Springer Undergraduate Mathematics Series*, 2010.

[22] D. Fabozzi and T. Van Cutsem, "Simplified time-domain simulation of detailed long-term dynamic models," in *2009 IEEE Power Energy Society General Meeting*, pp. 1–8, 2009.

[23] M. O. Donovan, N. Barry, and J. Connell, "Distance protection of transmission lines connected to inverter-based resources," in *2023 58th International Universities Power Engineering Conference (UPEC)*, pp. 1–6, 2023.

[24] J. L. Blackburn and T. Domin, "Protective relaying : Principles and applications, fourth edition," 1997.

[25] H. Holttinen, J. Kiviluoma, D. Flynn, J. C. Smith, A. Orths, P. B. Eriksen, N. Cutululis, L. Söder, M. Korpås, A. Estanqueiro, J. MacDowell, A. Tuohy, T. K. Vrana, and M. O'Malley, "System impact studies for near 100% renewable energy systems dominated by inverter based variable generation," *IEEE Transactions on Power Systems*, vol. 37, no. 4, pp. 3249–3258, 2022.

[26] B. Kroposki, C. Pink, R. DeBlasio, H. Thomas, and M. Simões, "Benefits of power electronic interfaces for distributed energy systems," *IEEE Transactions on Energy Conversion*, vol. 25, pp. 901–908, 2010.

[27] "IEEE draft standard for interconnection and interoperability of inverter-based resources (ibr) interconnecting with associated transmission electric power systems," *P2800/D6.3, December 2021*, pp. 1–181, 2021.

[28] M. Hossain, S. M. Boyer, S. C. Brown, and T. H. Nguyen, "Inverter-based generation integration protection challenges: Real-life experiences," *2023 76th Annual Conference for Protective Relay Engineers (CFPR)*, pp. 1–4, 2023.

[29] Y. Levron, J. Belikov, and D. Baimel, "A tutorial on dynamics and control of power systems with distributed and renewable energy sources based on the dq0 transformation," *Applied Sciences*, 2018.